Spatially Resolved Derivatization of Solid-Phase-Synthesis Beads with Fluorescent Dendrimers: Creation of Localized Microdomains

by **Claudia M. Cardona**, **Stephan H. Jannach**, **Hao Huang**[1]), **Yukiko Itojima**[1]), **Roger M. Leblanc**, and **Robert E. Gawley***

Department of Chemistry, and Marine and Freshwater Biomedical Sciences Center, University of Miami, P. O. Box 249118, Coral Gables, Florida, 33124-0431, USA (phone: +1 305 284 3279; fax: +1 305 668 3313; e-mail: rgawley@miami.edu)

and

Gary A. Baker and **Eric B. Brauns**

Los Alamos National Laboratory, Michelson Resource, Bioscience Division, P.O. Box 1663, Mail Stop J586, Los Alamos, NM 87545, USA

Dedicated with congratulations and best wishes to Professor *Dieter Seebach* on the occasion of his 65th birthday! Thanks for all you have done for organic chemistry in general, and organic synthesis in particular.

Second and third generation *Newkome*-type trifurcated dendrimers, containing either a coumarin or dansyl fluorescent probe at the dendrimer core, have been synthesized and attached to ArgoGel® solid-phase-synthesis beads. Subsequent reaction with rhodamine dye shows that the dye can penetrate throughout the beads to acylate the remaining sites. Thus, it is possible to achieve a spatially resolved microdomain for library formation at the core of the dendrimer, primarily on the bead's periphery, and a second microdomain suitable for derivatization by other reagents such as encoding tags and fluorescent sensors.

Introduction. – Dendrimers are highly branched, monodisperse polymers composed of well-organized structures [1]. *Fig. 1,a* illustrates a generic, third-generation trifurcated dendrimer showing the core and peripheral regions. Initially, research on dendrimers focused on their synthesis and on examination of their physical properties. More recently, efforts have shifted to finding applications that take advantage of their novel properties. The dendritic framework isolates sites in the interior of the dendrimer with characteristic nano-environments [2]. In fact, molecular probes located at the core of the dendrimer display physical properties that are modulated by their encapsulation within the periphery (for a few examples, see [3]). On the other hand, the high degree of branching gives rise to a periphery with many terminal groups, which can be derivatized for a variety of purposes (for a few examples, see [4]).

In the past several years, dendrimer chemistry has found applications in the field of solid-phase synthesis. Dendrimers may be synthesized on solid support or attached to a solid support to increase the loading capacity of a resin (*Fig. 1,b*) [5]. Similarly, grafted dendrimers may be employed as heterogeneous catalysts and reagents [5g,h], or chiral stationary phases for chromatography [5a].

---

[1]) *H. H.* on leave from Shanghai Institute of Organic Chemistry, China; *Y. I.* on leave from Kagoshima University, Japan.

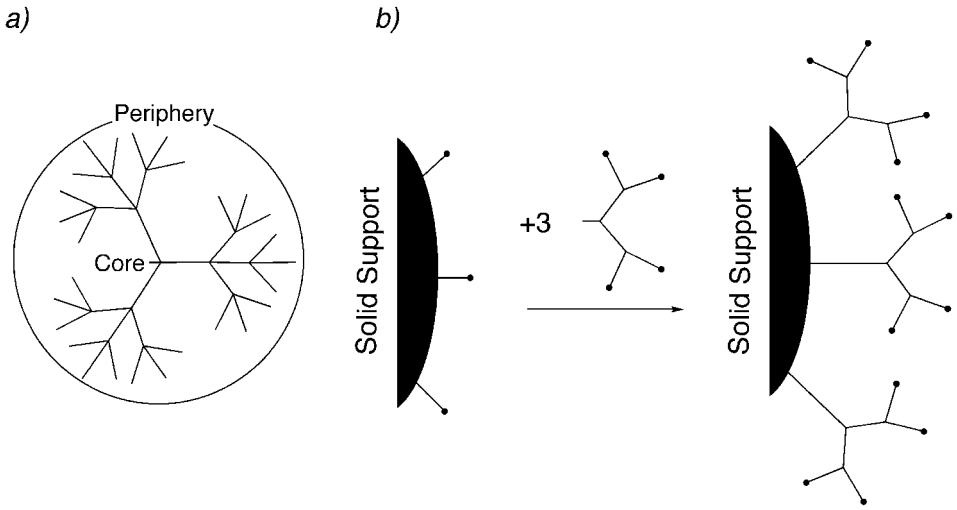

Fig. 1. a) *A generic backbone of a trifurcated dendrimer such as those presented in this paper, showing how the periphery encapsulates the core.* b) *Attachment of a bifurcated dendron to active sites on a solid support increases the number of active sites for solid-phase synthesis or conversion to multiple catalytic sites.*

In pioneering work, *Seebach et al.* have incorporated TADDOL, a versatile chiral ligand [6], at the core of an aromatic *Fréchet*-type dendrimer suitable for use as a cross-linking co-polymer in the preparation of polystyrene beads having the dendritic chiral ligand embedded throughout the solid support (*Fig. 2*) [7]. After introduction of a titanium, these heterogeneous catalysts perform extremely well when compared with their homogeneous counterparts. The chiral ligands BINOL and Salen may be embedded in a similar fashion, thus establishing the generality of this strategy for heterogeneous catalysis [8].

Our work is aimed at combinatorial design of dendritic mimics of receptor proteins and enzymes attached to solid support. To date, we have used 'rational' design to prepare a series of fluorescent sensors for the marine toxin saxitoxin [9], but we are also

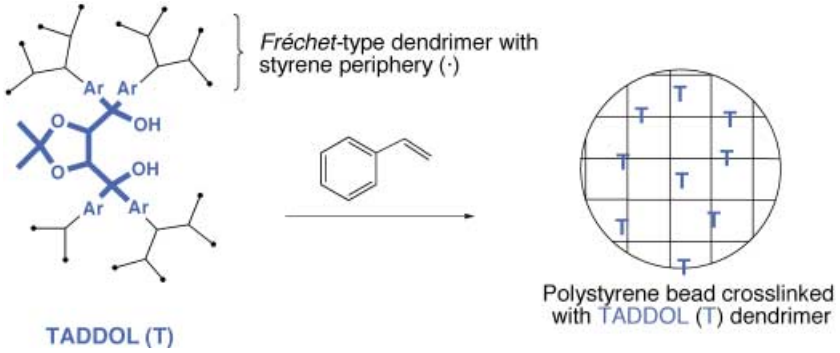

Fig. 2. *TADDOL Ligands* (T), *where the aryl groups are* Fréchet-*type dendrimers having styryl groups on the periphery, may be copolymerized to incorporate the TADDOL moiety throughout the polymer resin* [7].

interested in encapsulating a sensor within a dendrimer. We reason that the proteinogenic receptors of xenobiotics such as saxitoxin are enclosed within an (at least partially) solvent-excluded binding site [10], and that, perhaps, locating a receptor/sensor in a similarly solvent-excluded dendrimer would enhance binding and/or selectivity and/or sensitivity. Moreover, similar reasoning could be applied to the design of enzyme mimics.

To use combinatorial techniques in this effort, we have developed methodology for the synthesis and attachment of trifurcated *Newkome*-type dendrimers to solid support. Herein, we show, by incorporation of a fluorescent dye at the core of both two- and three-generation dendrimers, by epifluorescence and laser-scanning confocal microscopy, that the dendrimer does not acylate all the active sites in and on the bead, leaving numerous sites unreacted and, therefore, available for further derivatization (*Fig. 3*).

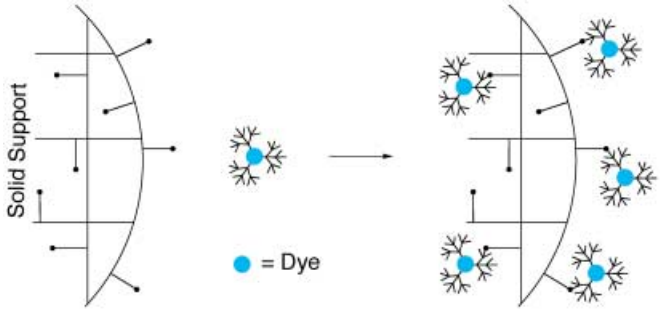

Fig. 3. *Cartoon representation of attachment of a dye-containing dendrimer to only some of the active sites in a polymer resin*

To obtain a high degree of encapsulation in the smallest number of generations, we decided to prepare *Newkome*-type trifurcated dendrons, based on a tris core [11], but with *t*-Bu end-groups to maximize spreading in the second- and third-generation. The encapsulating effect is rapidly observed in the first three generations with trifurcated dendrimers [2a][3]. The specific dendrimers we targeted to attach to the solid support are shown in *Figs. 4* and *5*. Since our ultimate aim is to build combinatorial libraries at the core of the dendrimer, we wanted the more robust *tert*-butyl amides at the periphery instead of *tert*-butyl esters. For both the second (*Fig. 4*) and the third-generation dendrimers (*Fig. 5*), we wanted to evaluate different dyes for the different types of microscopy used to examine the distribution in the beads. '*Coumarin 343*' (=*2,3,6,7-tetrahydro-11-oxo-1*H,5H,*11*H-*[1]benzopyrano[6,7,8-*ij*]*quinolizine-9-carboxylic acid*) was selected because it is a visible fluorophore that can be excited with the 488-nm line of the Ar laser of a confocal microscope and is also suitable for use in epifluorescence microscopy. On the other hand, the dansyl (=5-(dimethylamino)-naphthalene-1-sulfonyl) fluorophore is unsuitable for confocal microscopy with a visible laser, but fluoresces when using epifluorescence microscopy. Also, it is less susceptible to self-quenching, when several fluorophores are in close proximity because of its large *Stokes*' shift (*ca.* 200 nm) [12].

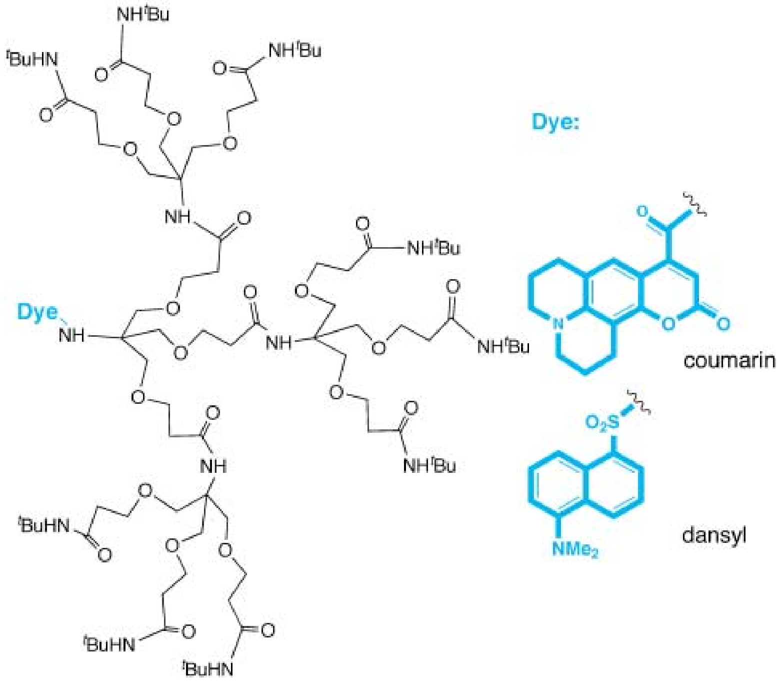

Fig. 4. *A second-generation* (G2) Newkome-*type dendrimer having a dye at the core*

Preparation of Fluorescent Dendrimers. – We have already reported a simple procedure for preparing the first- and second-generation dendrons needed [13]. *Scheme 1* shows the synthesis of the second-generation (G2) nona-acid dendrimer containing a coumarin fluorophore at the core. [(Benzyloxy)carbonyl]amino one-generation (G1) triacid **1** and amino G1 triester **2** were coupled with 1-ethyl-3-[3-(dimethylamino)propyl]carbodiimide (EDCI) in 76% yield to afford the [(benzyloxy)carbonyl]amino G2 nona-ester **3**. Removal of the (benzyloxy)carbonyl (Cbz) group by hydrogenolysis affords amino G2 nona-ester **4**. Coupling of amine **4** with 'coumarin 343' (**5**) with *O*-(1*H*-benzotriazol-1-yl)-1,1,3,3-tetramethyluronium hexafluorophosphate (HATU) afforded the G2 coumaryl nona-ester **6** in 77% yield, and removal of the nine *t*-Bu groups gave the G2 nona-acid **7** in quantitative yield. For simplicity, **7** will subsequently be illustrated as a set of two concentric circles, denoting the two generations of the dendrimer, with a cyan 'C' for the coumarin at the coumarin core, and with the nine carboxylic acid groups denoted as shown in the inset at the bottom of *Scheme 1*.

In a similar manner, the third-generation (G3) coumarin dendrimer was prepared as shown in *Scheme 2*. Triacid **1** and amino G2 nona-ester **4** were coupled to afford the Cbz G3 27-ester **8** in 56% yield. Hydrogenolysis gave the G3 amine **9** in 71% yield, and coupling with coumarin **5** afforded the coumaryl G3 27-ester **10** in 88% yield. Removal of the *t*-Bu groups was again quantitative and gave the G3 27-acid **11**, which will be written subsequently in cartoon form as three concentric circles and a cyan 'C' in the middle for coumarin, as shown in the inset.

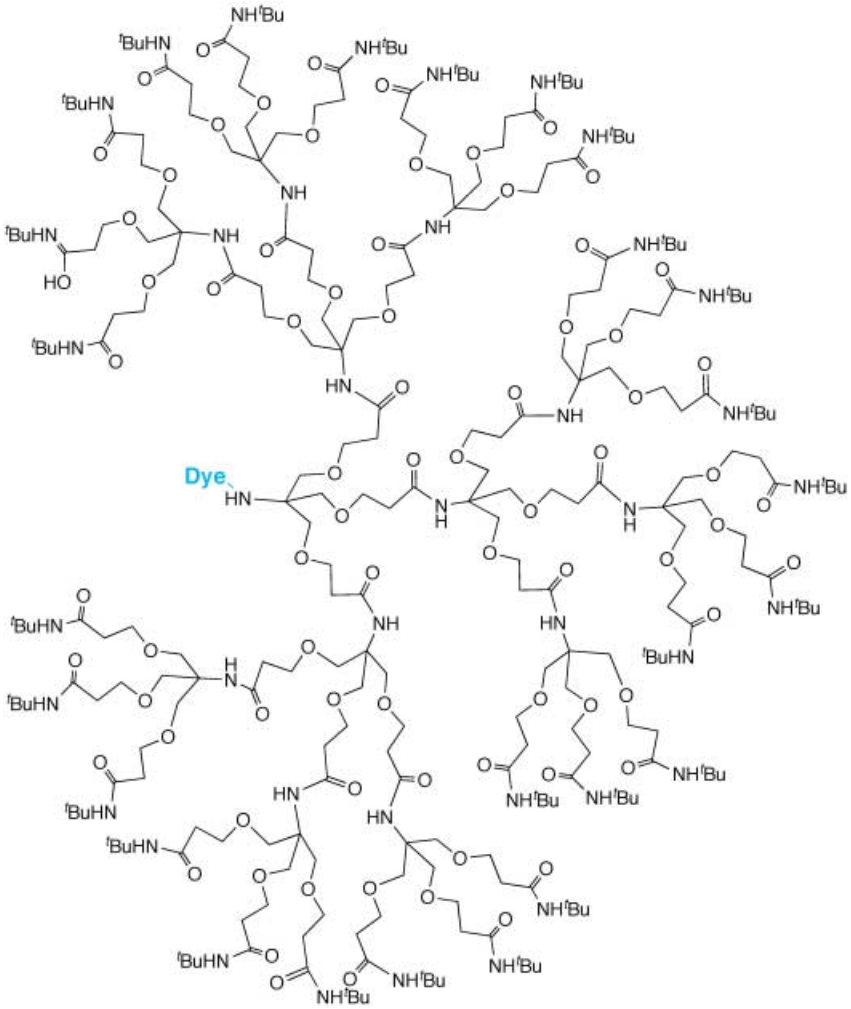

Fig. 5. *A third-generation* (G3) Newkome-*type dendrimer having a dye at the core.* Dyes as in *Fig. 4.*

The dendrimers containing a dansyl dye at the core were synthesized as shown in *Scheme 3*. In two steps, G1 amino triester **2** was acylated with dansyl chloride in 81% yield, and the *t*-Bu groups removed in 99% yield to afford G1 dansyl triacid **12**. This could be coupled to G1 amino-triester **2** to give the G2 nona-ester **13** in 82% yield. Removal of the *t*-Bu groups with HCOOH afforded the G2 nona-acid **14** in 93% yield. Nona-acid **14** could be coupled with G1 amino triester **2** to give the G3 27-ester **15** in 35% yield. Alternatively, G1 triacid **12** can be coupled with G2 amine **4** to afford **15** in 67% yield. Removal of the 27 *t*-Bu groups gives the G3 27-acid **16** in 89% yield.

It is interesting to note the different strategies for the synthesis of the coumarin dendrimers shown in *Schemes 1* and *2* with the strategy for the dansyl dendrimers in *Scheme 3*. Acylation of G1 triester **2** with coumarin **5** could be accomplished easily with

Scheme 1. *Synthesis of G2 Coumarin Nona-acid Dendrimer*

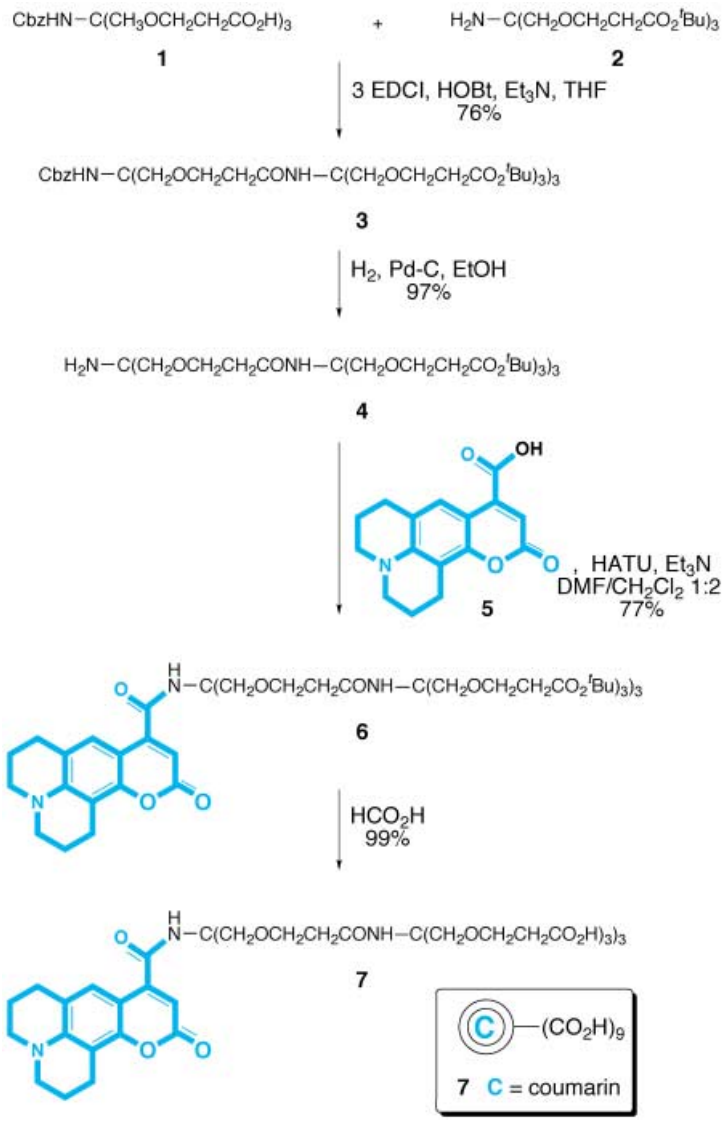

EDCI, but the resulting G1 coumaryl triester corresponding to **12** did not survive HCOOH treatment. In contrast, the coumaryl moiety of G2 nona-ester **6** and G3 27-ester **10** was quite stable to these conditions. This may be an example of the well-known dendritic effect [2a], whereby the periphery of the dendrimer encapsulates and protects functional groups at the dendritic core.

To attach the dendrimers to the resin beads, we planned to use carbodiimide coupling, followed by amidation with (*t*-Bu)NH_2 to introduce the robust, yet bulky

Scheme 2. *Synthesis of G3 Coumarin 27-Acid Dendrimer*

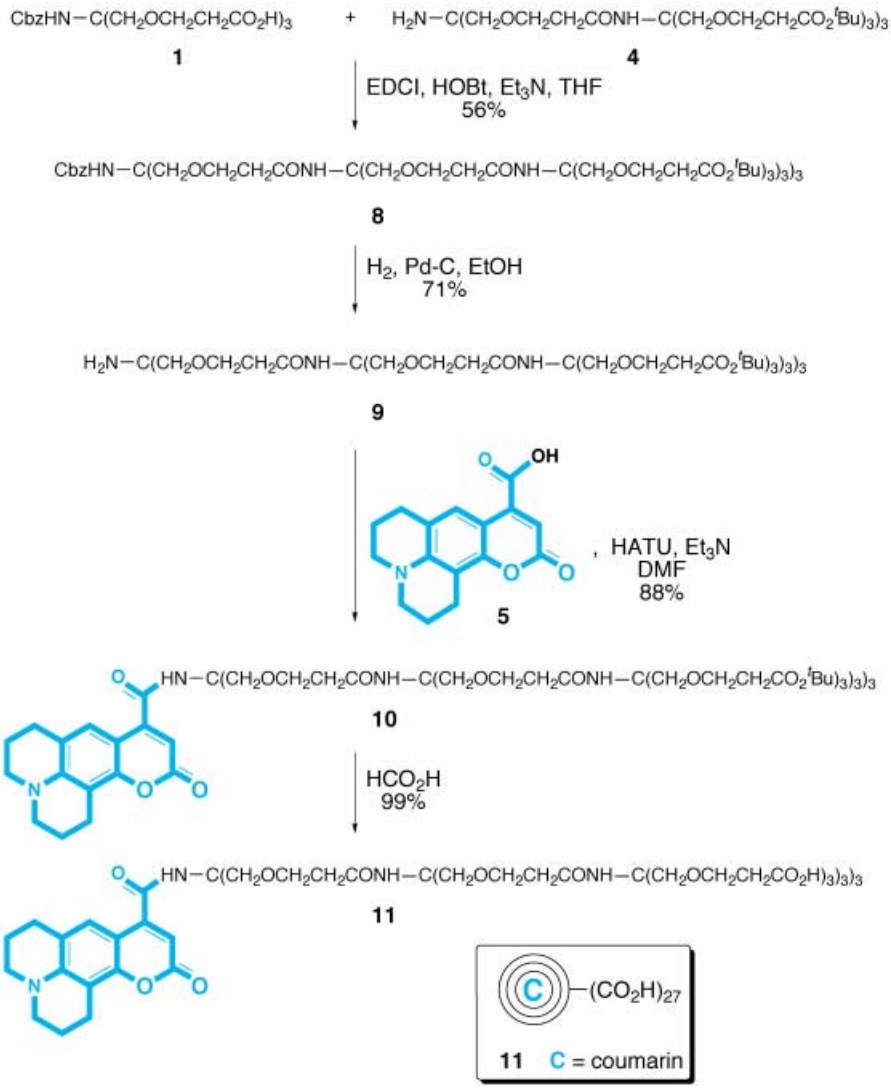

(*t*-Bu)NHCO functional group at the periphery. As control experiments to test the viability of functionalizing the periphery with (*t*-Bu)NH_2, we tested the reaction in solution phase as shown in *Scheme 4*. EDCI facilitated the coupling of Cbz G1 triacid **1** with (*t*-Bu)NH_2, which proceeded in 90% yield after column chromatography (*Scheme 4*,*a*). Similarly, as shown in *Scheme 4*,*b*, EDCI coupling of coumaryl G2 nona-acid **7** proceeded in 59% yield to give the coumaryl G2 nona-amide dendrimer **19a**, while diisopropyl carbodiimide (DIC) coupling of Cbz G2 nona-acid **18** afforded Cbz G2 nona-amide dendrimer **19b**, in 78% yield after chromatography. Although the NMR spectra of these dendrimers looked clean, the mass spectra showed minor

Scheme 3. *Synthesis of G2 and G3 Dansyl Nona- and 27-Acid Dendrimers*

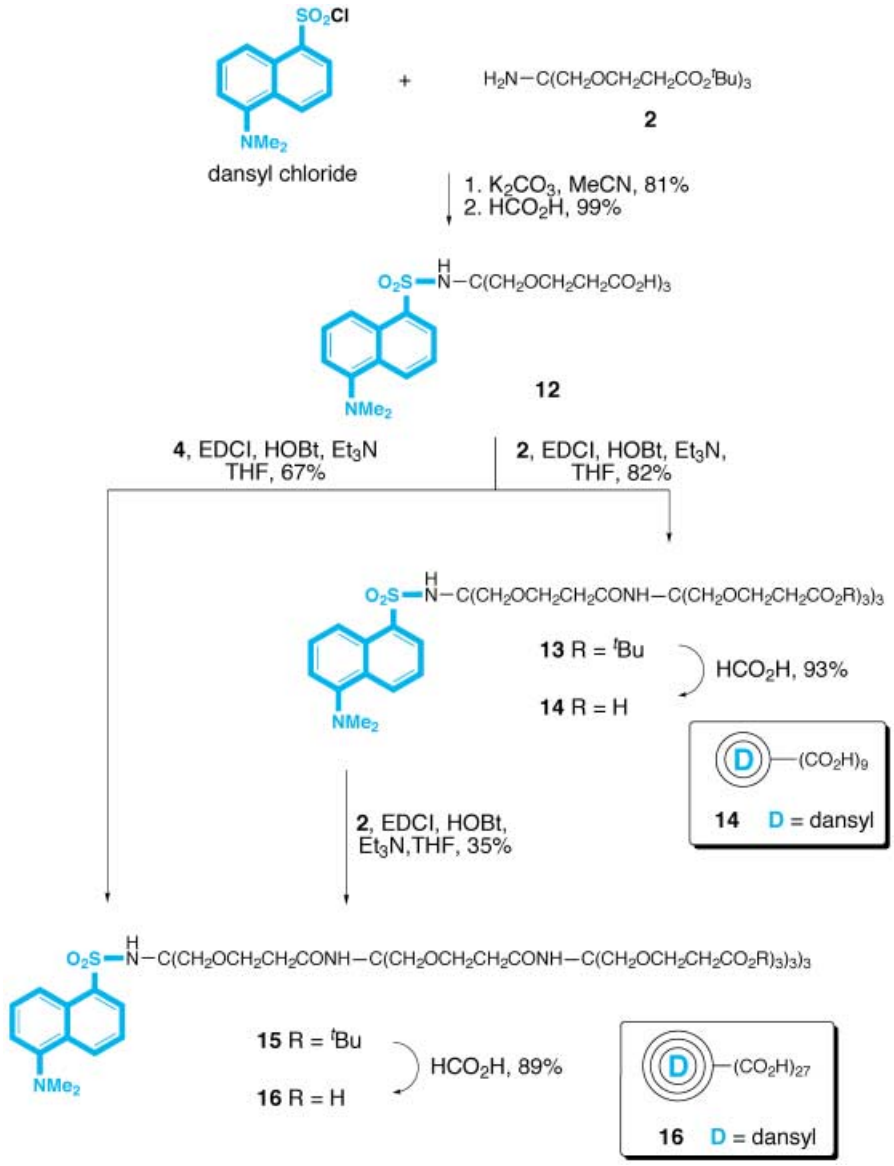

contamination with a dendrimer where one, and sometimes two, of the terminal carboxy groups are substituted with an *N*-acylurea, which resulted from rearrangement of the active ester.

Modification of ArgoGel-NH_2 Beads with Fluorescent Dyes. – ArgoGel® (*Argonaut Technologies*) beads are poly(ethylene glycol) (PEG) grafted onto

Scheme 4. *Synthesis of Nona-amide Dendrimers*

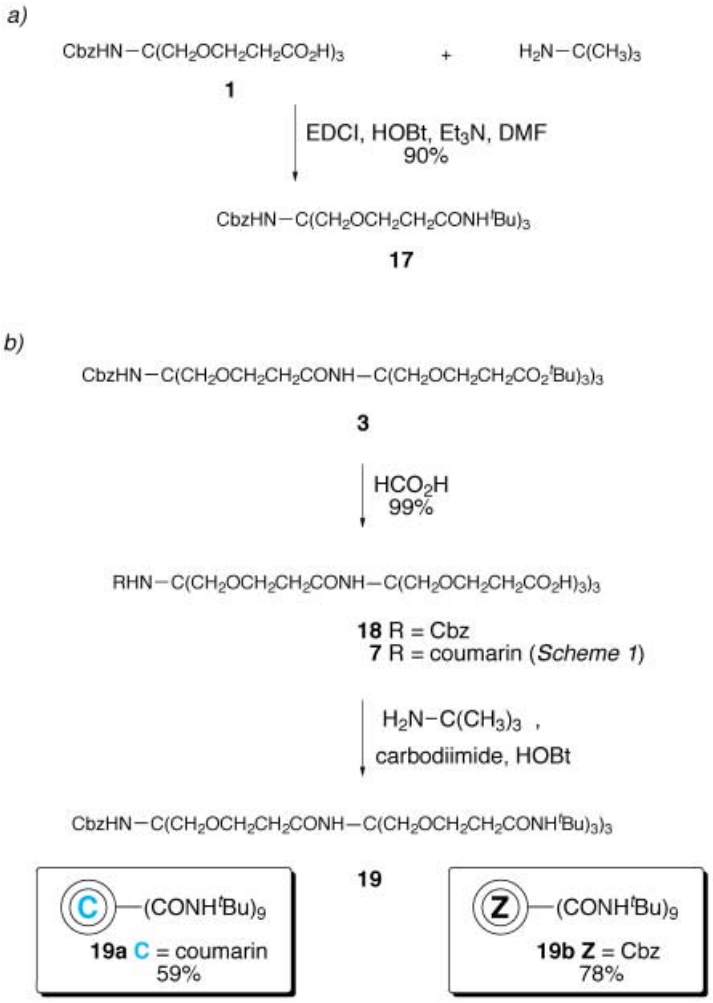

polystyrene and allow high loading due to a bifurcated polystyrene graft-linkage. The 'arms' of the PEG grafts, which have the active amine sites at their termini, impart enough flexibility that normal (*i.e.*, not solids probe) ^{13}C-NMR spectroscopy may be used to characterize the resin-bound products. *ArgoGel*® is also compatible with solvents ranging in polarity from H_2O to toluene. In this work, we employed *ArgoGel*-NH_2 resin with a 0.43-mmol/g loading and an average 164-μm diameter.

The nona-acid G2 coumarin, **7**, and dansyl, **14**, and the G3 27-acid coumarin, **11**, and dansyl, **16**, dendrimers were coupled to the *ArgoGel*® beads under standard peptide-coupling conditions, followed by amidation with (*t*-Bu)NH_2 to convert the unreacted active esters on the dendrimer to *N*-(*tert*-butyl) amides. These reactions afforded the G2 dye/dendrimer-bead conjugates **20** and **21**, and the G3 analogs **22** and **23**

(*Scheme 5*). In all cases, the stoichiometry of carboxy (on the dendrimer) to amine (on the resin) was set at 3:1. Because of the multifunctional nature of the dendrimers, the stoichiometry of dye to amine was 1:9 and 1:27 of this ratio, leaving the amine in 'molar' excess over the dendrimer. It is not known how many of the carboxy termini of the dendrimers reacted, hence the subscript '*n*' in structures **20**–**23**.

Scheme 5. *Attachment of G2 and G3 Coumarin and Dansyl Dendrimers to* ArgoGel® *Beads*

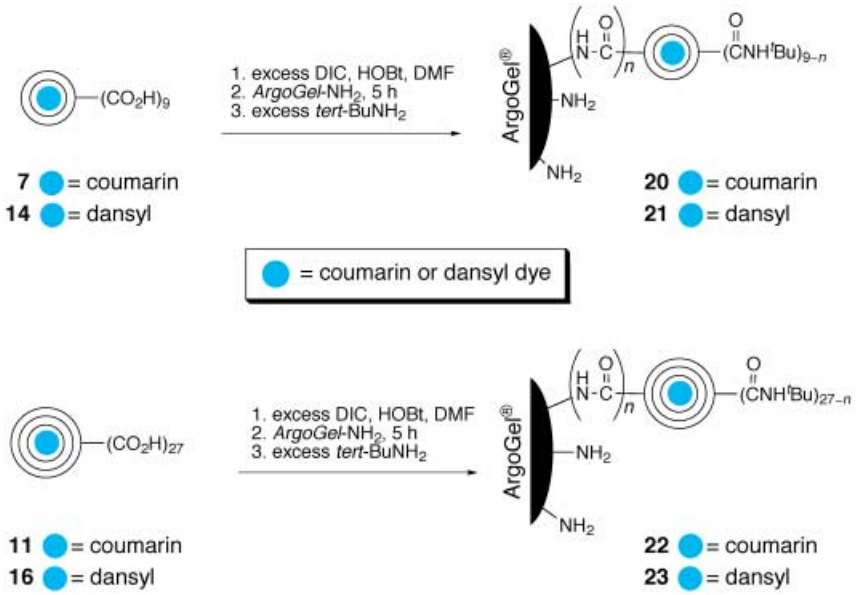

That both the coupling and the amidation were successful on the solid support is evident from a comparison of the ^{13}C-NMR spectrum of the independently prepared (homogeneous) sample of the coumaryl G2 nona-amide dendrimer **19a** with the analogous dendrimer **20** covalently bound to the bead (*Fig. 6*). In particular, note the four labeled signals in the spectrum, which belong to the indicated C-atoms in the second-generation (periphery) of the dendrimer. The chemical shifts are nearly identical, and the relative intensities suggest that the number of covalent linkages to the bead, *n*, is relatively small. In the spectrum of the dendrimer attached to the bead, the peak marked with a '*b*' is due to the resin. The small peaks marked with an '*x*' at 68 and 25 ppm, not seen in the upper spectrum or in the spectrum of the resin, are due to THF trapped in the resin or the dendrimer. These two peaks are significantly more prominent in the NMR spectrum of the G3 coumarin dendrimer **22** attached to the bead (not shown).

Because of the size of the G2 and G3 trifurcated dendrimers, we anticipated that diffusion through the dendritic matrix would be slowed relative to smaller molecules (even if they would fit!?), such that some of the active amine sites of the *ArgoGel*® resin, especially toward the middle of the bead, may not be accessible. To probe the distribution of possible unreactive sites, we selected beads modified with G2 and G3 coumarin dendrimers for further derivatization. For this, we selected rhodamine B, a

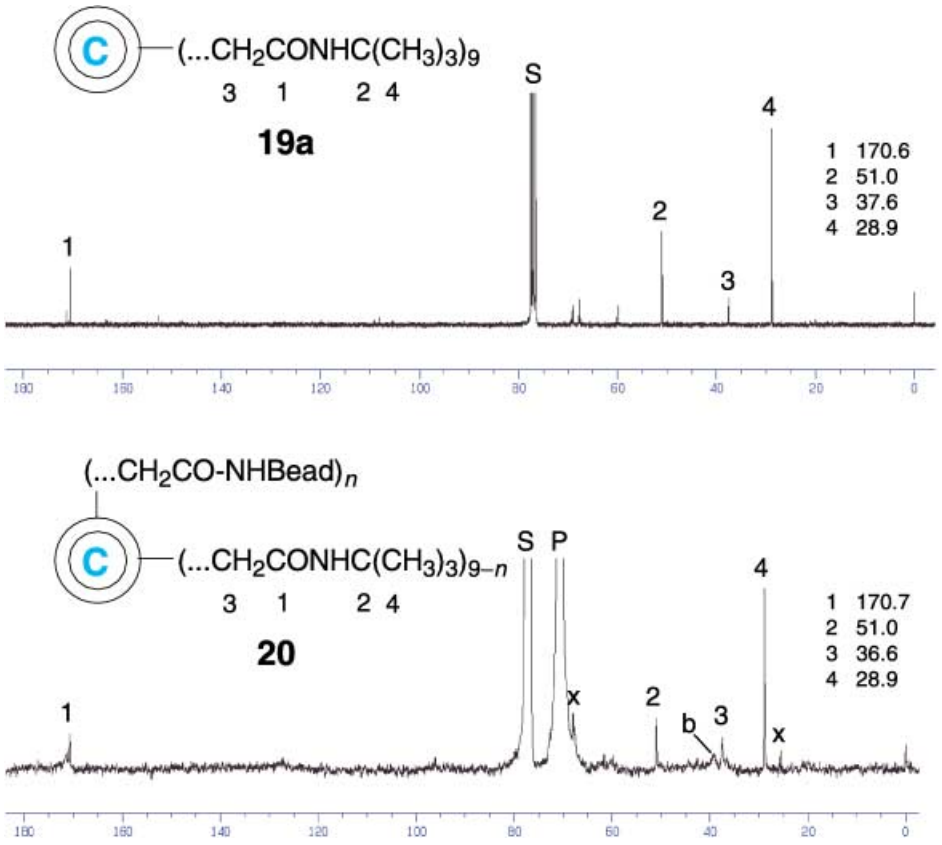

Fig. 6. a) *^{13}C-NMR Spectrum of* **19a**. S = $CDCl_3$. b) *^{13}C-NMR Spectrum of* ArgoGel® *beads with G2 coumaryl dendrimer covalently attached*; **20** (*Scheme 5* and text). S = $CDCl_3$; b = minor signal from resin; P = CH_2O C-atoms of polyethylene glycol (PEG) grafts on the resin; x = THF.

dye that fluoresces red instead of the blue-green of the coumarin dye. Moreover, the absorption maxima of these two dyes are sufficiently far apart (*ca.* 440 nm for coumarin and *ca.* 540 nm for rhodamine) that the two dyes can be excited selectively with appropriate filters in an epifluorescence microscope.

The phenomenon of fluorescence quenching in epifluorescence microscopy has been addressed in both whole beads [12] and slices made with a microtome [14], as well as in confocal microscopy [14]. We did not anticipate that this phenomenon would be important, when the dye was encapsulated in a dendrimer, but in the absence of the dendrimer, we wanted to avoid the issue. Therefore, we diluted the rhodamine B isothiocyanate reagent with 27 equiv. of cyclohexyl isothiocyanate. As shown in *Scheme 6*, the G2 coumarin-modified bead, **20**, and the G3 coumarin-modified bead, **22**, were treated with a mixture of isothiocyanates to afford triply derivatized resins **24** and **25**, respectively. The distribution of the two dyes throughout the beads were determined by epifluorescence microscopy as described in a later section. In the structures of **24** and **25**, '*n*' has the same meaning as it has in *Scheme 5:* the number of

Scheme 6. *Attachment of Rhodamine Dye to G2 and G3 Coumaryl Dendrimer Beads*

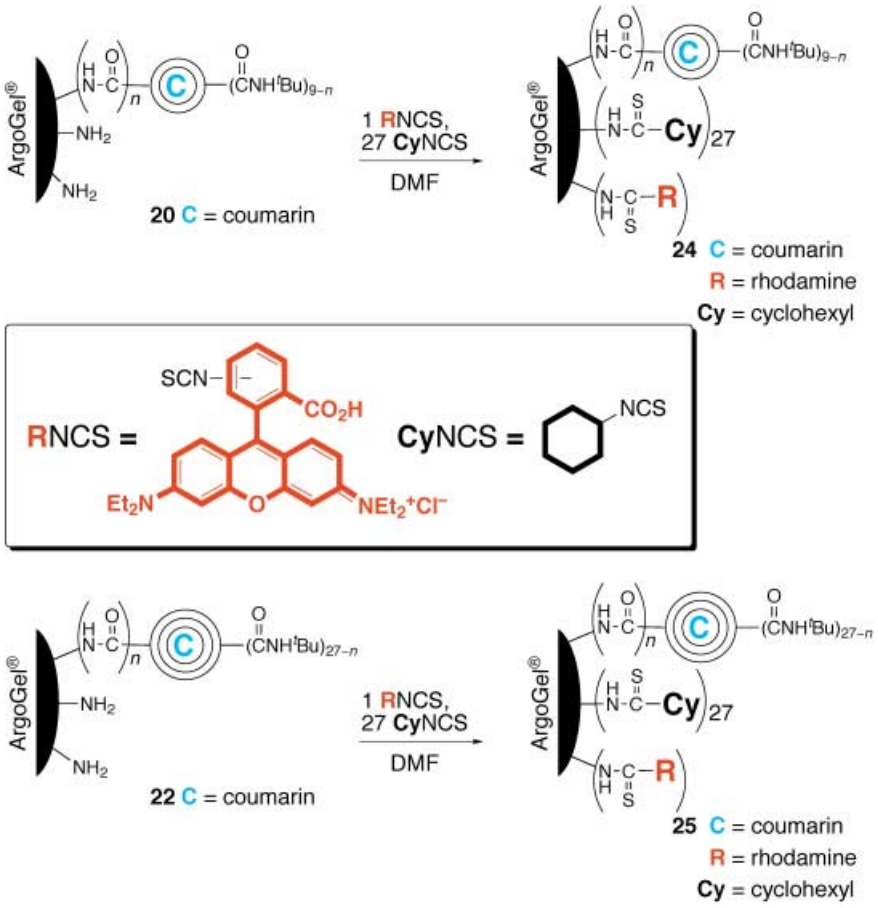

dendritic termini covalently linked to the resin. The ratio of cyclohexyl to rhodamine modified sites is 27 : 1, but the ratio of dendrimer sites to the cyclohexyl/rhodamine sites is not known.

As controls for the microscopy experiments described below, we also prepared beads containing the coumarin and dansyl fluorophores, without the dendrons, in order to visualize the distribution of the active sites throughout the beads and to test for any self-quenching between proximal fluorophores in or on the bead. As depicted in *Scheme 7*, two sets of beads were modified with only the fluorophores, either coumarin **5** or dansyl chloride, to label every available amino group throughout the bead (*i.e.*, **26** and **27**). We also prepared beads with coumarin **5** and cyclohexanecarboxylic acid in 1 : 9 and 1 : 27 proportions, **28** and **29**, respectively. The role of the cyclohexanecarboxylic acid, a non-fluorescent molecule, is to dilute the fluorophore throughout the resin to prevent self-quenching by proximal fluorophores on solid support [12][14][15]. Note that all the beads were derivatized under very similar conditions. The only

Scheme 7. *Attachment of Pure and Diluted Dyes to* ArgoGel® *Beads*

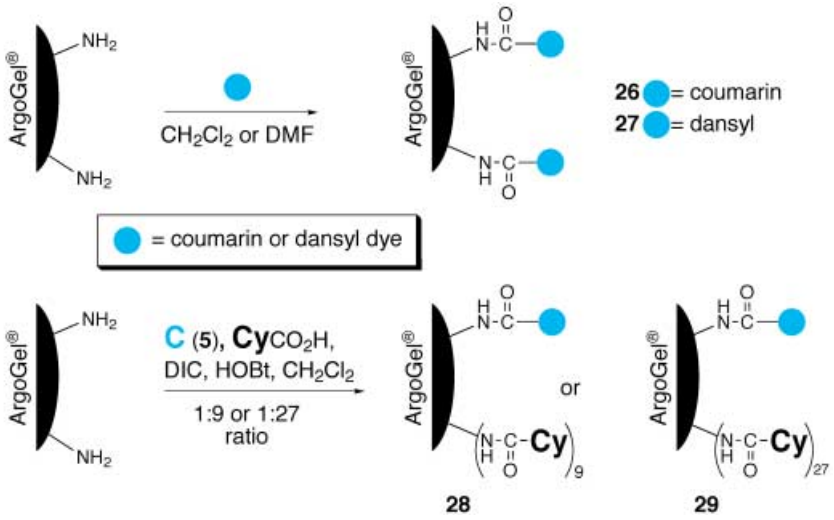

difference was the solvent employed, since coumarin **5** is very soluble in CH_2Cl_2 and only slightly in DMF, and the resin swells similarly in both solvents[2]).

Fluorescence Studies of Dendritic Beads. – Three types of microscopy were used in this work. Laser-scanning confocal microscopy (LSCM), which focuses a laser on a plane that penetrates intact resin beads, was used to semiquantitatively assess the distribution of coumarin fluorophores throughout the interior of beads. Because of the wavelength of the laser (488 nm), this technique was limited to beads containing the coumarin fluorophore. The colors seen in the LSCM images are false color images that reflect the intensity of emitted light: red is brightest and blue is the most dim. Epifluorescence microscopy (EFM) was used to evaluate the distribution of coumarin, dansyl, and rhodamine fluorophores on beads after they had been physically sliced into wafers *ca.* 3–5-μm thick. Environmental-scanning electron microscopy (ESEM) was used to evaluate the morphology of whole beads and selected wafers. The ESEM images were taken in a water vapor atmosphere at low vacuum. The surfaces have not been modified by sputtering of a heavy metal.

Fig. 7 shows LSCM and ESEM images of clusters of *ArgoGel*® beads modified with the G3 coumarin/dendrimer-bead conjugate (*i.e.*, **22**). In the LSCM image on the left, which represents a plane slicing through the center of the beads, note the uneven distribution of emitted light throughout the beads, as well as localized spots of more intense (red) emission on the periphery of some of the beads. In the ESEM image on the right, note that all of the beads show defects in the surface, including craters and, in some cases, pieces that have been gouged from the surface but are still attached[3]). We

[2]) *Argonaut Technologies* product specification for *ArgoGel*®.

[3]) Such defects are the result of the manufacturing process. Beads taken straight from the jar contain similar deformities.

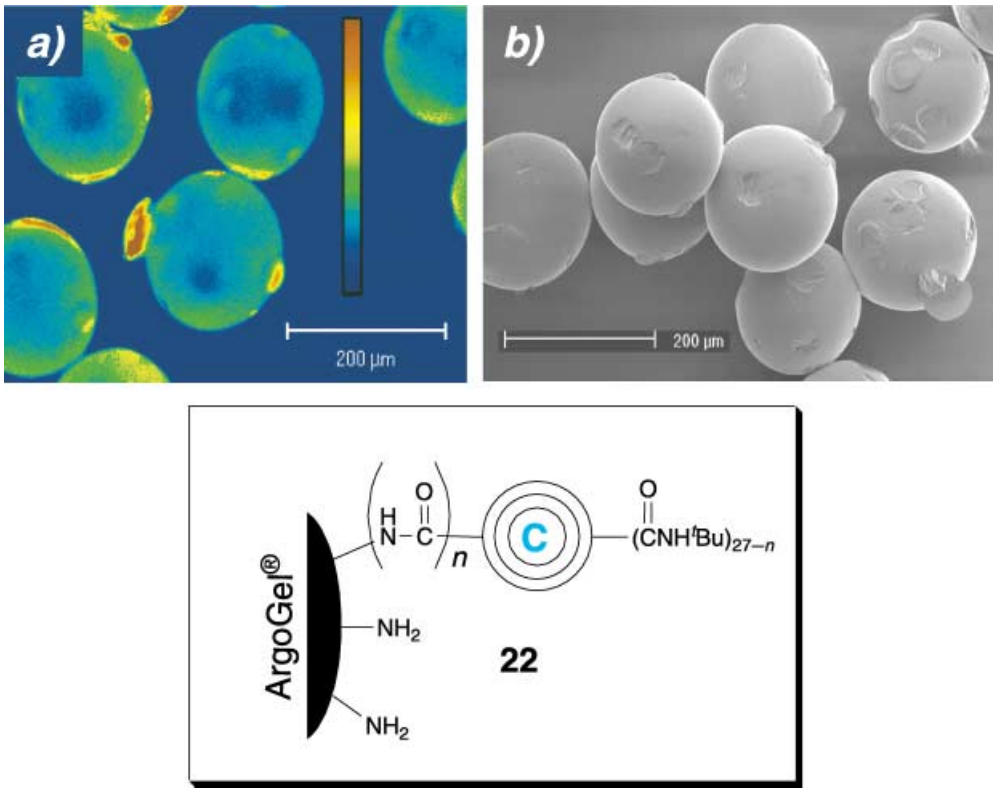

Fig. 7. a) *LSCM Image* (10× objective) *of a plane bisecting a group of G3 dendrimer beads* **22** (false color shows relative intensity of emitted light: red is brightest). b) *ESEM Image of* **22**.

believe that the bright red spots in the LSCM image correspond to the type of defect shown in the ESEM image.

LSCM can acquire successive 'optical slices' across successive planes in individual beads, and, therefore, provide a '*z*-scan' that maps fluorescence intensity in planes dissecting the bead at different 'latitudes'. *Fig. 8* shows such a *z*-scan for bead **22**. At this magnification (40×), each optical slice corresponds to a thickness of *ca.* 1–2 µm. Note that the slices nearest the middle of the bead, *A* and *B*, are similar to the images in *Fig. 7*, and show high concentrations of fluorophore near the periphery and lower concentrations in the interior. Successive slices show varying distribution patterns of fluorophore. Near the top of the bead, slices *C* and *D*, the fluorophore appears to be more evenly distributed across each slice.

Fig. 9,a shows the LSCM image of another coumarin/dendrimer bead **22**; the diameter of the image (black line), 166 µm, corresponds closely to the diameter of the bead, and, therefore, this optical slice is near the center of the bead. In this image, there is clearly a higher concentration of the dendritic fluorophore near the edge of the bead, and significantly less emission from the central region, although the distribution in the middle is far from homogeneous. Defects in the bead are discernable at the top and right sides of the bead. *Fig. 9,b* shows a semiquantitative profile of intensity of emitted

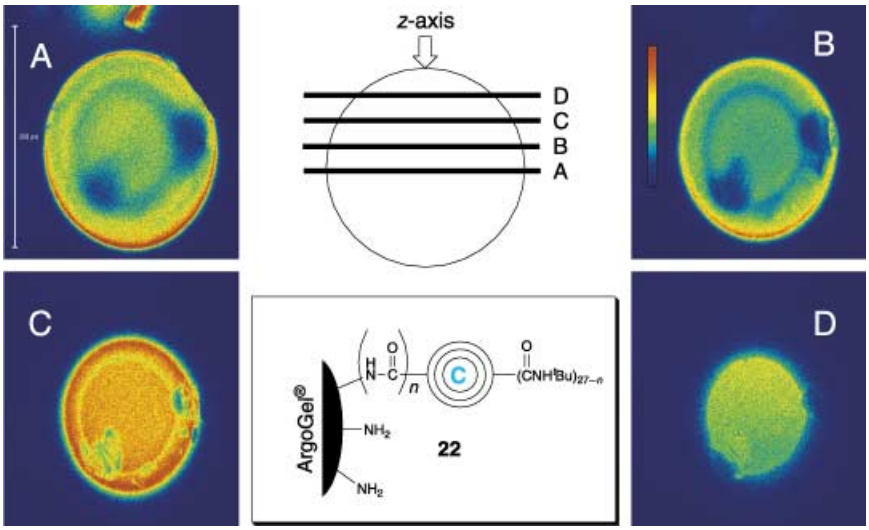

Fig. 8. *LSCM* z*-Scan of G3 coumaryl-dendrimer bead* **22**. The figure in the center shows the direction of view of the LSCM image, and the black lines indicate the dissecting planes corresponding to the four images shown.

light recorded along the path indicated by the white arrow in *Fig. 9*,*a* and clearly shows higher intensity at the bead's edge. *Fig. 9*,*c* and *d* show EFM and ESEM images of a cluster of three wafers, *ca.* 5-μm thick, cut from three G3 coumarin/dendrimer beads, **22**, that were stuck together. In the image in *Fig. 9*,*c*, the color is real, and corresponds to the fluorescence of the coumarin dye at the core of the attached dendrimer. Again, higher concentrations near the periphery of each wafer are evident. The ESEM image in *Fig. 9*,*d*, of the same three wafers, shows how slicing by a microtome produces a rather uneven surface when cutting through the polystyrene matrix[4]), with a tear evident in the lower left, and holes in two of the wafers. In *Fig. 9*,*e*, a wafer cut from a G3 dansyl/dendrimer bead, **23**, shows a layer of thin, 'crusty' emission at the edge of the bead, reminiscent of the solar corona, but otherwise even distribution of fluorophore across the wafer. Control experiments (*vide infra*) show that this 'corona' is an artifact, and is not indicative of a microdomain. With the dansyl fluorophore within the dendrimer, the emission intensity is considerably less, and long exposures (up to several seconds) were necessary to record an image.

Similar experiments were performed with the G2 coumarin/dendrimer, **20**, and G2 dansyl/dendrimer, **21**, beads. *Fig. 10*,*a* shows a LSCM optical slice near the center of a bead, and *Fig. 10*,*b* shows the profile of emission intensity taken along the direction of the white arrow. The similarity of these images to the images of the G3 dendrimer beads (*Fig. 9*,*a* and *b*) is striking. It would appear from these images that, again, the dendrimer is not distributed uniformly throughout the beads. However, an EFM photograph of a 5-μm wafer, *Fig. 10*,*c* shows considerably less contrast between the interior and the periphery than the EFM images in *Fig. 9*,*c*. EFM Photographs of the

[4]) The wafers sliced by the microtome are far from uniform. See *Exper. Part.*

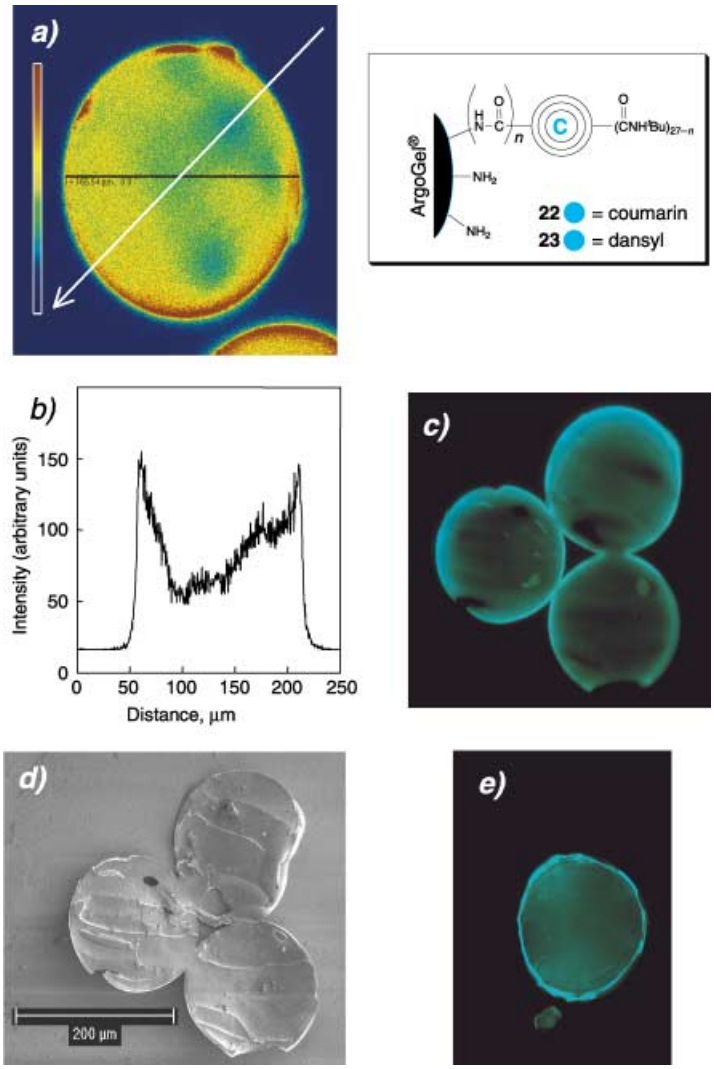

Fig. 9. a) *LSCM Image of the center of G3 coumarin/dendrimer bead* **22**. b) *Profile showing intensity of emitted light along path of white arrow in* a. c) *EFM Image of three microtome wafers,* ca. *5-µm thick, of G3 coumarin/dendrimer bead* **22**. d) *ESEM Image of the same wafers in* c. Note the curled corrugated surface and holes in two of the wafers. e) *EFM Image of a microtome wafer of G3 dansyl/dendrimer bead* **23**.

G2 dansyl/dendrimer beads **21** (again requiring a long exposure time) also show little discernable contrast (*Fig. 10*,*d*)[5]). Taken together, these images suggest that the G2

[5]) In EFM, the entire specimen is irradiated with UV light, and the resulting fluorescence originates from throughout the specimen, including above and below the plane of focus. This superimposition obscures structural details that might otherwise be resolved. In addition, for specimens thicker than the depth of field (such as these wafers), light from out-of-focus planes may create diffuse halos around objects of study, degrading contrast.

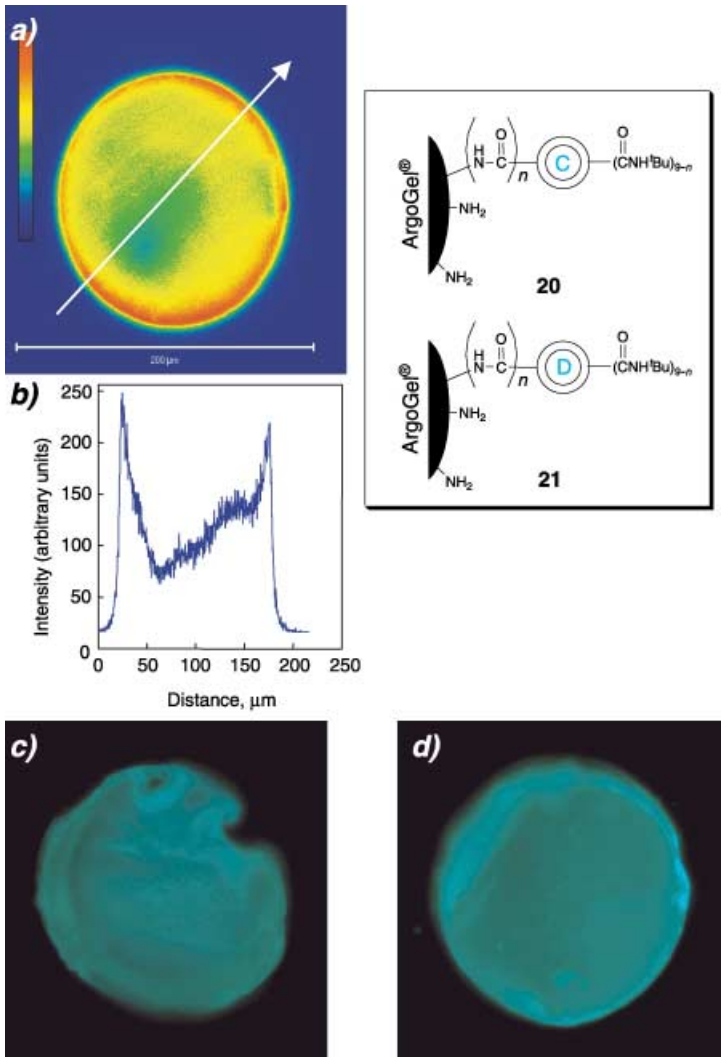

Fig. 10. a) *LSCM Image of the center of G2 coumarin/dendrimer bead* **20**. b) *Intensity profile of emitted light along path of white arrow in* a. c) *EFM Image of a wafer,* ca. *5-µm thick, of G2 coumarin/dendrimer bead* **20**. d) *EFM Image of a microtome wafer of G2 dansyl/dendrimer bead* **21**.

dendrimer penetrates the bead more effectively than the G3. The higher concentration of fluorophore at the periphery evident in the LSCM image may be due, in part, to a higher concentration of active sites on and near the bead's exterior (see also the control experiments below).

The data presented so far strongly suggest that the dendrimer-fluorophores do not occupy all the sites in the bead. Indeed, it appears that the G3 dendrimers attach selectively on or near the periphery of the bead. Since the dendrimer is added in a substoichiometric amount relative to active amine, this makes sense due to the

presumably slow diffusion rate of the larger dendrimer through the polymer matrix. The converse of this situation is that there should be numerous unreacted sites, and that most of them should be in the interior portion of the beads. Thus, beads modified as outlined in *Scheme 6* were sliced and examined for the distribution of coumarin *vs.* rhodamine dyes, using filters that selectively excite one fluorophore over the other. *Fig. 11*,*a* shows two images of the same wafer of a G3 coumarin/dendrimer bead that is also modified with a 1:27 mixture of rhodamine B and a nonfluorescent cyclohexyl dilutant (**25**; see *Scheme 6*)[6]). In the upper image, fluorescence of the G3 coumarin/

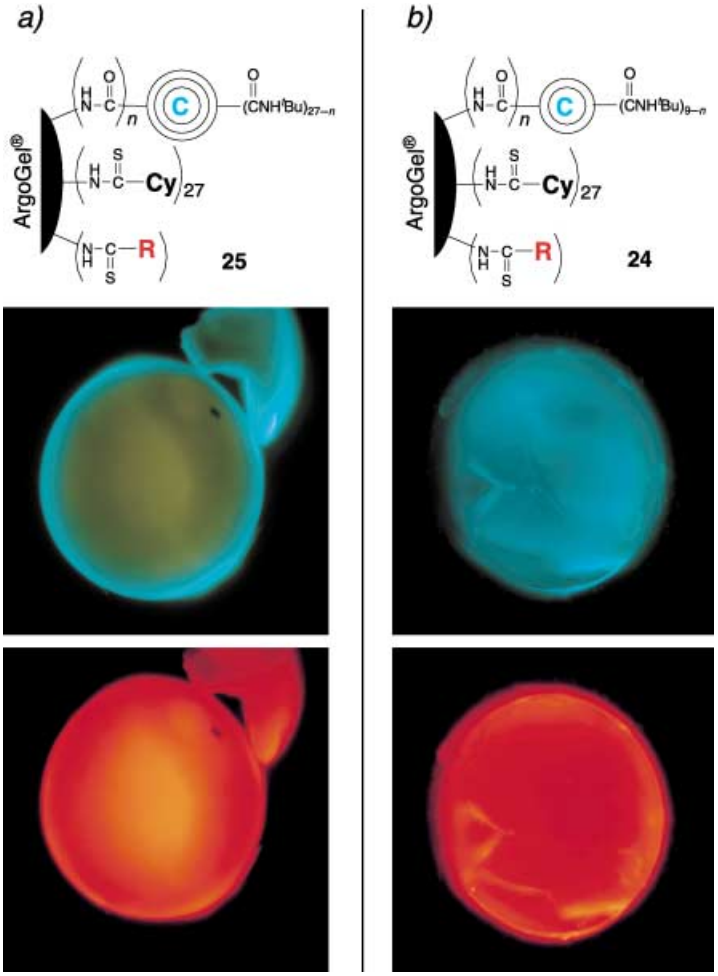

Fig. 11. a) *EFM Images of a microtome wafer of G3 coumaryl dendrimer/rhodamine bead* **25**. b) *Similar Images of G2 coumaryl dendrimer/rhodamine bead* **24**. For both beads, the upper image is taken with a BV filter block: excitation 400–440 nm, barrier 470 nm. The lower image is taken with a G filter block: excitation 510–560 nm, barrier 590 nm. See *Exper. Part.*

[6]) The cyclohexyl dilutant is to prevent proximal quenching of the rhodamine fluorophore in the polymer matrix [12]. The *Stokes*' shift of rhodamine is only *ca.* 20–25 nm, depending on substituents.

dendrimer is clearly visible primarily around the periphery of the wafer, whereas, in the lower image, the rhodamine is present throughout. The contrasting region in the upper image is curious, and may be the result of energy transfer from coumarin to rhodamine chromophores, or 'bleeding through' of some rhodamine fluorescence in microdomains where it is more prevalent. *Fig. 11,b* shows similar images of the G2 coumarin/dendrimer bead, modified with rhodamine, **24**. In this case, distribution of both fluorophores is evident throughout the bead.

Thus, with reference to the method of preparation illustrated in *Scheme 6*, the rhodamine dye is clearly able to penetrate throughout the resin, past and through both the G2 and G3 dendrimers. Thus, it is possible to achieve a spatially resolved microdomain with G3 dendrimers attached to the bead's periphery, with an interior microdomain suitable for derivatization by other reagents. Even when diffusion throughout the bead occurs with the G2 dendrimer, many unreacted sites remain. This may mean that not all sites are accessible to the G2 dendrimer. In related work, *Miller* and co-workers recently demonstrated that beads can be partitioned into as many as five spatially resolved microdomains by using the kinetics of diffusion of small molecule reagents into the core of the resin bead [16]. In our work, we made no attempt to determine the kinetics of diffusion.

Controls. – Several papers in the recent literature have addressed the issue of fluorophores on solid support from a number of perspectives [12][14][17]. For example, *McAlpine et al.* used the distribution of fluorophore to evaluate the distribution of active sites throughout the resin bead [17][7]). However, since, to our knowledge, there are no reports on *ArgoGel*®, we used LSCM and EFM to examine fluorophore-derivatized beads *lacking dendrimers,* described above in *Scheme 7. Fig. 12* shows a comparison of *ArgoGel*® that has been saturated with 100% coumarin (*i.e.*, **26**) with 10% coumarin/90% cyclohexane (*i.e.*, **28**), and with 4% coumarin/96% cyclohexane (*i.e.*, **29**). *Fig. 12,a* shows the all-coumarin bead. The LSCM optical slice at the top, and the intensity profiles in the middle show clear diminution of emission from the center of the bead. The EFM image of the wafer at the bottom also shows darkening in the interior of the wafer. *Fig. 12,b* shows that, when the fluorophore is diluted with a derivatizing agent lacking a chromophore, an even distribution of chromophore can be seen in both the optical slice, its intensity profile, and the microtome slice at the bottom.

Consistent with previous observations [12][14], we believe that the lack of fluorescence in the center of bead **26** is due to self-quenching by proximal chromophores, when all sites are occupied. Active sites are closer together in the center of the bead[8]). When the fluorophore is diluted such that only 10% of the active sites have fluorophore, self-quenching is eliminated, and emission is uniform across the polymer matrix.

Further dilution of fluorophore, as shown in *Fig. 12,c*, produced a surprise. In particular, the optical slice now shows a predominance of fluorophore at the periphery and even distribution of fluorophore throughout the interior. Note that the intensity of

---

[7]) Some of the conclusions of this report have been challenged [14].

[8]) On the surface of the bead, active sites are distributed in two dimensions. In the interior, they are distributed in three dimensions.

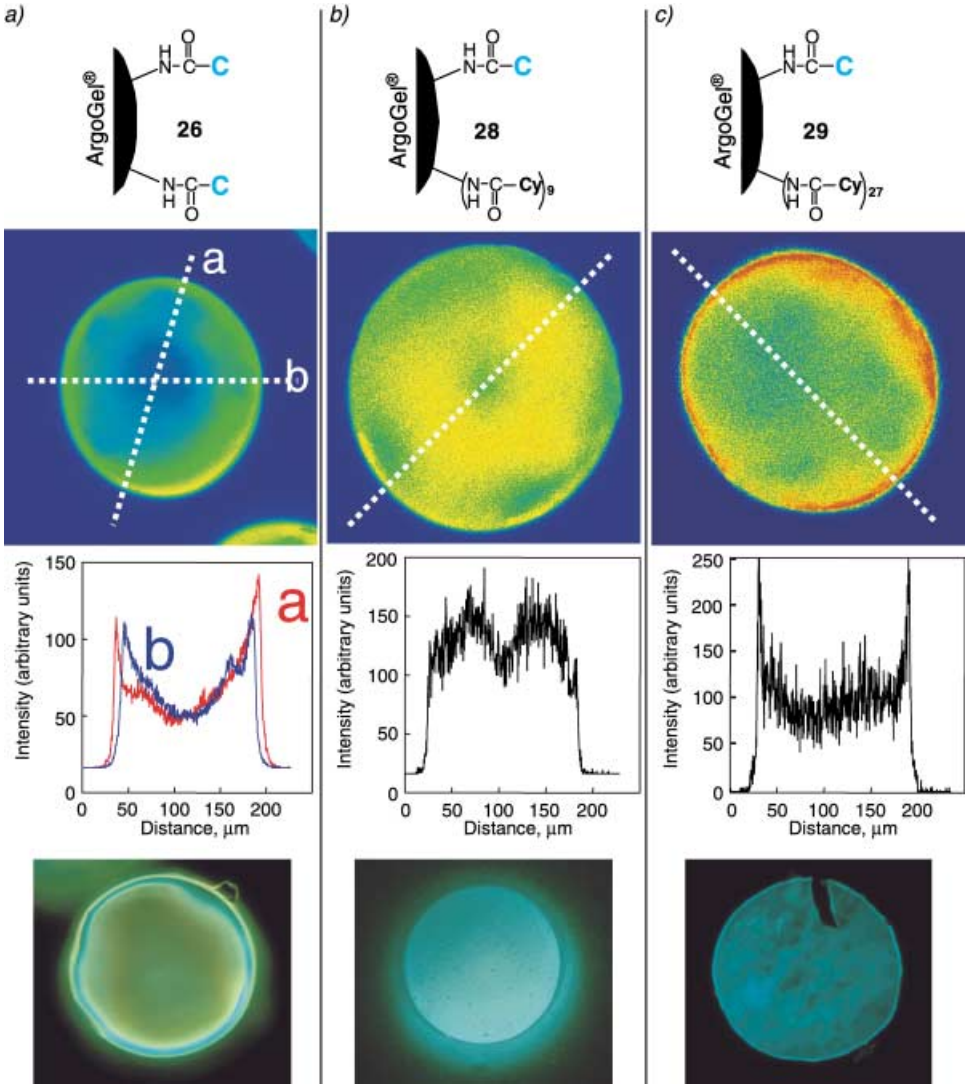

Fig. 12. *Images of coumarin-modified beads, as described in* Scheme 7. *Top:* Confocal image through center of bead. *Middle:* Profile of intensity of emitted light in confocal image. *Bottom:* Epifluorescence image of 5-µm wafer from center of beads. a) *All-coumarin bead* **26**. b) *Coumarin/cyclohexyl 1*:*9 bead* **28**. c) *Coumarin/cyclohexyl 1*:*27 bead* **29**.

emission, as judged by the noise in the intensity profile, is rather low, and the difference in intensity is not great. We speculate that there is a sufficiently low concentration of fluorophore on the bead that stronger emission is only visible where there are high concentrations of active sites on the resin. In the EFM image at the bottom, a weak fluorescence emission across the diameter of the wafer is evident; the light 'crusty' edge, reminiscent of the 'corona' in *Fig. 9*,*e*, is an artifact due to the curling of the edge

producing light refraction[5]). The EFM image of a wafer cut from the all-dansyl modified bead **27** (*Scheme 7*) is indistinguishable from that of **29**.

Conclusions. – We have shown that *ArgoGel®* beads can be partially derivatized with G2 or G3 *Newkome*-type dendrimers, while, at the same time, leaving active sites within the resin untouched and accessible by other reagents.

Our results show that the confocal and epifluorescence microscopy are useful techniques for locating functionalized sites on solid-support, given the appropriate precautions to avoid self quenching of a fluorophore. Derivatization with coumarin requires dilution to avoid self-quenching, but derivatization with dansyl does not [12].

In our work, the presence of the unmodified amine sites in the dendritically modified beads produces spatially resolved microdomains that can be differentially functionalized and visualized by epifluorescence microscopy. Thus, dendrimer-modified sites can play one role while other sites remain available for other uses such as encoding [18] or sensing [15].

We are grateful to Dr. *John Berry* for help with the epifluorescence microscopy, to Dr. *Matt Lynn* for running the ESEM experiments, to Mr. *Alix Vieux* and Dr. *Spencer Howell* for help with the microtome slicing, and to Ms. *Sara Hinds* for assistance with some of the synthesis and chromatography. Financial support from the *US Department of Agriculture* (USDA No. 0191270), and core support from the *Marine and Freshwater Biomedical Sciences Center* by NIEHS-NIH (ES 05705) is gratefully acknowledged. *C. M. C.* thanks NIEHS-NIH (ES 05931) for an individual fellowship. The contents of this paper are solely the responsibility of the authors and do not necessarily represent the official views of the NIEHS, NIH. Finally, we are very grateful to Prof. Dr. *Steve Miller* and Mr. *Gary Copeland* (Boston College) for much helpful advice on epifluorescence microscopy.

Experimental Part

General. All commercially available reagents were purchased from *Aldrich* or *Acros*, and were used without further purification unless otherwise noted. THF was distilled from sodium benzophenone ketyl, and CH_2Cl_2 was distilled from CaH_2 or stirred over basic alumina and filtered. Column chromatography (CC) was performed on silica gel *60* (230–400 mesh), while TLC was carried out using aluminum-backed plates coated with 0.25-mm silica gel *60* (*F-254*). UV/VIS Spectra were obtained with a *Shimadzu* model *2101* double-beam spectrometer equipped with a cell-holder kept at 25°. The spectra are reported as λ_{max}, nm (ε, $M^{-1}cm^{-1}$). Steady-state fluorescence spectra were recorded with a *Spex Fluoromax* system and used uncorrected. For epifluorescent spectroscopy, see below. NMR Spectra were recorded on 400- or 300-MHz instruments, and chemical shifts (δ) are reported in ppm with either Me_4Si or residual solvent as internal reference, as noted. *J* values are reported in Hz. Mass spectra (MS) of compounds with a molecular weight below 2000 amu were recorded by FAB on a *VG* single-stage quadrupole mass spectrometer. Mass spectra for compounds with a molecular weight above 2000 amu were obtained by a *Bruker MALDI-TOF* spectrometer (positive-ion mode; matrix as indicated), respectively. *Atlantic Microlab Inc* carried out elemental analyses.

Epifluorescence microscopy was performed with an inverted *Nikon TS100-F* microscope (10×, 20×, and 40× objectives) with a *C-SHG* epifluorescence unit and three *Nikon* filter blocks: a standard *UV-1A* filter was used for the dansyl fluorophore (excitation 330–380 nm, barrier 420 nm), standard *BV-2A* filter for the coumarin 343 fluorophore (excitation 400–440 nm, barrier 470 nm), and a standard *G-2A* filter for the rhodamine B fluorophore (excitation 510–560 nm, barrier 590 nm). Photographs were recorded with a *Nikon CoolPix 990* Digital camera mounted to a trinocular photo tube. Exposure times for the dansyl fluorophore were 1/2 to 2 s in duration. Exposure times for the courmarin 343 fluorophore were 1/1000 to 1/250 s and for the rhodamine B fluorophore 1/15 to 1/4 s.

Laser-scanning confocal microscopy (LSCM) was performed with a *Zeiss Axiovert 100M* inverted microscope coupled to a *Zeiss LSM 510* scanning module. Excitation at 488 nm was provided by an air-cooled argon-ion laser (*ca.* 10–15 mW). 'Survey' scans (*e.g.*, *Fig. 7,a*) were collected with a 10× plan-neofluar (0.3 NA) objective and subsequent higher-resolution scans (all others) used a 40× *LD-achroplan* (0.6 NA)

microscope objective. In all cases, the coumarin emission was collected by a 488 dichroic mirror and passed through a 505-nm longpass filter. The typical pinhole setting was varied from 50–100 μm, corresponding to 1.5–2.5-μm thick optical sections. Images were typically acquired in 1–2 s, resulting in a pixel dwell time of 4–8 μs for the frame size used (512–512). For all samples, the detector gain was adjusted to effectively fill the 8-bit A/D board.

Scanning electron microscopy (SEM) was performed with a *Philips/Electroscan ESEM FEI-XL30* field-emission-gun environmental SEM. The images of the beads and microtome slices were obtained in a low vacuum SEM mode with a (1.00–1.40 keV) electron beam. Beads were mounted on a SEM sample holder with double-stick carbon tape. The microtome slices in *Fig. 9,d* were mounted on a glass microscope slide.

*Syntheses. 2,3,6,7-Tetrahydro-11-oxo-*N*-{tris[(2-{[(tris{[2-(*tert*-butoxycarbonyl)ethoxy]methyl}methyl)-amino]carbonyl}ethoxy)methyl]methyl}-1*H,5H,*11*H*-[1]-benzopyrano[6,7,8-*ij*]quinolizine-9-carboxamide* (**6**). Compound **5** (0.10 g, 0.35 mmol) was dissolved in 2 ml of anh. DMF and 5 ml of anh. CH_2Cl_2. Then, Et_3N (0.12 ml, 0.86 mmol) and HATU [19] (0.14 g, 0.37 mmol) were added, and the mixture was allowed to stir for 5 min under N_2. Thereafter, compound **4** [13], dissolved in 5 ml of CH_2Cl_2, was added, and the mixture was stirred for 24 h at r.t. Then, the solvent was removed under vacuum, and the residue was purified by CC (SiO_2; AcOEt/hexane 2:1 to 100:0). An orange-yellow, viscous oil was obtained (0.58 g, 77%). UV/VIS (MeOH): 437 (3.4×10^4), 268 (9.4×10^3). ^{1}H-NMR (400 MHz, $CDCl_3$): 1.44 (*s*, 27 Me); 2.45 (*m*, 12 CH_2); 2.76 (*t*, $J = 6.0$, CH_2); 2.86 (*t*, $J = 6.4$, CH_2); 3.32 (*dd*, $J = 6.4$, 2 CH_2); 3.63 (*t*, $J = 6.4$, 9 CH_2); 3.70 (*m*, 12 CH_2); 3.80 (*s*, 3 CH_2); 6.13 (*s*, 3 NH); 6.97 (*s*, NH); 8.52 (*s*, NH). ^{13}C-NMR ($CDCl_3$, 75 MHz): 20.14; 20.29; 21.22; 27.46; 28.12; 36.18; 37.53; 49.79; 50.21; 59.76; 60.07; 67.04; 67.72; 69.16; 69.39; 80.38; 105.61; 108.25; 110.21; 119.38; 126.95; 147.55; 147.87; 152.67; 162.69; 162.87; 170.86; 170.89. MALDI-MS (anthracene): 2089 ($[M + Na]^+$). Anal. calc. for $C_{104}H_{171}N_5O_{36}$ (2067.48): C 60.42, H 8.34; found: C 60.50, H 8.37.

*2,3,6,7-Tetrahydro-11-oxo-*N*-{tris[(2-{[(tris{[2-carboxyethoxy]methyl}methyl)amino]carbonyl}ethoxy)methyl]methyl}-1*H,5H,*11*H*-[1]benzopyrano[6,7,8-*ij*]quinolizine-9-carboxamide* (**7**). Compound **6** (0.28 g, 0.13 mmol) was stirred in 15 ml of 96% HCOOH for 26 h at r.t. The reaction was monitored by TLC, and, upon completion, the HCOOH was removed under vacuum. Any remaining traces of HCOOH were removed by dissolving the product in MeOH and evaporating *in vacuo*. The product was dried under vacuum at r.t. for 18 h. A dark-brown, viscous, and hydroscopic oil was recovered (0.20 g, 99%). ^{1}H-NMR (300 MHz, CD_3OD): 1.99 (*m*, 2 CH_2); 2.49 (*m*, 12 CH_2); 2.79 (*m*, CH_2); 2.84 (*m*, CH_2); 3.38 (*m*, 2 CH_2); 3.68 (*m*, 2 CH_2); 3.82 (*s*, 3 CH_2); 7.13 (*s*, CH); 8.49 (*s*, CH); 9.27 (*s*, NH). ^{13}C-NMR (75 MHz, CD_3OD): 36.01; 38.44; 61.64; 68.35; 69.06; 70.23; 174.17; 175.85. FAB-MS: 1563 ($[M + H]^+$), 1297 ($[M -$ coumarin$]^+$), 1154 ($[M - C_{16}H_{26}NO_{11}]^+$). Anal. calc. for $C_{68}H_{99}N_5O_{36} \cdot 3\ H_2O$ (1616.57): C 50.52, H 6.55; found: C 50.83, H 6.77.

Benzyl N*-Tris({2-[({tris[(2-{[(tris{[2-(*tert*-butoxycarbonyl)ethoxy]methyl}methyl)amino]carbonyl}-ethoxy)methyl]methyl}amino)carbonyl]ethoxy}methyl)methylcarbamate* (**8**). Compound **1** [13] (0.058 g, 0.12 mmol) was combined with HOBt (0.016 g, 0.12 mmol) in 3.0 ml of anh. THF, and the mixture was cooled to 0° in an ice-bath. Then, EDCI (0.079 g, 0.41 mmol) was added followed by Et_3N (0.060 ml, 0.41 mmol) and **4** [13] (0.74 g, 0.41 mmol) in 3.0 ml of anh. THF. At this point, 2.0 ml of THF were used to transfer any residual **4** into the reaction flask. The temp. was allowed to slowly rise to r.t., and the mixture was allowed to stir under N_2 for 4 d. After removing the solvent under reduced pressure, the residue was dissolved in Et_2O, and washed with 0.5M HCl and brine. The org. layers were dried ($MgSO_4$), and the solvent was removed *in vacuo*. The crude product was then purified by CC (SiO_2; AcOEt/MeOH 100:0 to 99:1) to yield a colorless viscous oil (0.41 g, 56%). ^{1}H-NMR (300 MHz, (D_6)acetone): 1.46 (*s*, 81 Me); 2.43 (*m*, 39 CH_2); 3.67 (*m*, 78 CH_2); 5.08 (*m*, CH_2); 6.02 (br. *s*, NH); 6.63 (br. *s*, 9 NH); 6.78 (br. *s*, 3 NH); 7.41 (*m*, 5 CH). ^{13}C-NMR (100 MHz, (D_6)acetone): 28.55; 36.96; 37.91; 60.08; 60.88; 60.96; 68.03; 68.53; 68.76; 69.98; 70.19; 80.63; 128.66; 128.82; 129.37; 171.31; 171.41; 171.52. MALDI-MS (anthracene): 5841 ($[M + Na]^+$). Anal. calc. for $C_{285}H_{497}N_{13}O_{107}$ (5818.02): C58.84, H 8.61; found: C 58.76, H 8.79.

*Tris({2-[{[tris-({2-{[(tris{[2-(*tert*-butoxycarbonyl)ethoxy]methyl}methyl)amino]carbonyl}ethoxy}methyl)methyl]amino}carbonyl]ethoxy}methyl)methylamine* (**9**). Compound **8** (0.23 g, 0.039 mmol) was stirred with 10% Pd/C (0.024 g) in EtOH (10 ml) under H_2 at r.t. for 48 h. The mixture was filtered over *Celite* and through a 0.2-μm *Millipore* filter. The solvent was removed under reduced pressure at 50°, and a colorless oil was recovered (0.16 g, 71%). ^{1}H-NMR (400 MHz, (D_6)acetone): 1.46 (*s*, 81 Me); 2.45 (*m*, 39 CH_2); 3.35 (*s*, 3 CH_2); 3.67 (*m*, 75 CH_2); 6.66 (br. *s*, 9 NH); 6.80 (br. *s*, 3 NH). ^{13}C-NMR (100 MHz, (D_6)acetone): 28.55; 36.96; 37.89; 60.69; 68.03; 68.54; 69.89; 69.97; 80.64; 171.43; 171.54. MALDI-MS (anthracene): 5685 ($[M + H]^+$).

*2,3,6,7-Tetrahydro-11-oxo-*N*-{tris({2-({[tris({2-{[(tris{[2-(*tert*-butoxycarbonyl)ethoxy]methyl}methyl)amino]carbonyl}ethoxy}methyl)methyl]amino}carbonyl)ethoxy]methyl)methyl}-1*H,5H,*11*H*-[1]benzopyrano[6,7,8-*ij*]quinolizine-9-carboxamide* (**10**). Compound **5** (0.0095 g, 0.033 mmol) was dissolved in 5 ml of anh. DMF and

the soln. was cooled to 0° in an ice-bath under N_2. Then, Et_3N and HATU [19] were added, and the soln. was allowed to stir for 5 min before the G3 amino 27-*tert*-butyl ester, **9**, dissolved in 2 ml of anh. DMF, was added. An additional 3 ml of DMF were used to transfer the amine to the reaction vessel. The mixture was allowed to reach r.t. slowly, and it was stirred for 5 d. Subsequently, the DMF was distilled off under reduced pressure, and the residue was purified by CC (SiO_2; AcOEt/MeOH 100:0 to 90:10). A viscous dark orange oil was obtained (0.15 g, 88%). IR (CH_2Cl_2): 1727 (C=O, ester), 1675 (C=O, amide). ^{1}H-NMR (300 MHz, $CDCl_3$): 1.39 (*s*, 81 Me); 1.73 (*m*, 2 CH_2); 2.38 (*m*, 39 CH_2); 2.70 (*m*, CH_2); 2.80 (*m*, CH_2); 3.25 (*m*, 2 CH_2); 3.63 (*m*, 78 CH_2); 5.95 (br. *s*, 3 NH); 6.05 (br. *s*, 9 NH); 6.94 (*s*, CH); 8.46 (*s*, CH); 9.03 (br. *s*, NH). ^{13}C-NMR (75 MHz, $CDCl_3$): 28.14; 36.17; 37.29; 59.81; 67.06; 67.59; 69.16; 80.40; 170.40; 170.78; 170.89. MALDI-MS (anthracene): 5948 ($[M+H]^+$), 2193 ($[M+Na-2\,C_{92}H_{164}N_4O_{35}]^+$). Anal. calc. for $C_{293}H_{504}N_{14}O_{108}$ (5947.44): C 59.13, H 8.54; found: C 59.08, H 8.50.

2,3,6,7-Tetrahydro-11-oxo-N-*{tris([2-({[tris({2-{[(tris{[2-carboxyethoxy]methyl}methyl)amino]carbonyl}-ethoxy}methyl)methyl]amino}carbonyl)ethoxy]methyl)methyl}-1*H,5H,*11*H-*[1]benzopyrano[5,7,8*-ij*]quinolizine-9-carboxamide* (**11**). Compound **10** (0.11 g, 0.018 mmol) was stirred in 15 ml of 96% HCOOH for 48 h at r.t. The HCOOH was then removed *in vacuo*, and any traces of remaining acid were removed by co-distilling with MeOH under vacuum. The product was allowed to dry at 40° for 8 h *in vacuo*. A dark-brown, viscous, and extremely hygroscopic oil was recovered (0.081 g, 99%). ^{1}H-NMR (300 MHz, CD_3OD): 1.89 (*m*, 2 CH_2); 2.41 (*m*, 39 CH_2); 2.75 (*m*, 2 CH_2); 3.62 (*m*, 78 CH_2); 7.08 (*s*, CH); 8.45 (*s*, CH); 9.17 (*s*, NH). ^{13}C-NMR (75 MHz, CD_3OD): 36.10; 38.30; 61.70; 68.42; 69.00; 70.26; 174.19; 175.86. MALDI-MS (DHB): 4451 ($[M+H+H_2O]^+$), 4469 ($[M+H+2\,H_2O]$)$^+$, 4472 ($[M+K+H_2O]$)$^+$, 4490 ($[M+K+2\,H_2O]^+$), 4508 ($[M+K+2\,H_2O]^+$), 4526 ($[M+K+3\,H_2O]^+$), 3068 ($[M-C_{55}H_{89}N_4O_{35}]^+$), 3086 ($[M-C_{55}H_{89}N_4O_{35}+H_2O]^+$), 3104 ($[M-C_{55}H_{89}N_4O_{35}+2\,H_2O]^+$), 3122 ($[M-C_{55}H_{89}N_4O_{35}+3\,H_2O]^+$). Anal. calc. for $C_{185}H_{288}N_{14}O_{108}\cdot 8\,H_2O$ (4580.42): C 48.51, H 6.69; found: C 48.57, H 6.67.

5-(Dimethylamino)-N-*{tris[(2-carboxyethoxy)methyl]methyl}naphthalene-1-sulfonamide* (**12**). Dansyl chloride (0.53 g, 2.0 mmol), **2** [13] (0.57 g, 1.1 mmol), and K_2CO_3 anh. (0.57 g, 4.0 mmol) were stirred in 10 ml of anh. MeCN under N_2 at r.t. for 36 h. The mixture was filtered, and the solvent was removed under reduced pressure. The residue was purified by CC (SiO_2; hexane/AcOEt 4:1) to give slightly green solid (dansyl G1 triester; 0.73 g, 81%). The dansyl G1 tri-(*tert*-butyl) ester (0.50 g, 0.67 mmol) was stirred in 8 ml 96% HCOOH under N_2 at r.t. for 24 h. The HCOOH was removed under reduced pressure. Any traces of HCOOH were removed by dissolving the product in $CHCl_3$ and evaporating *in vacuo* to give a slightly yellow foam (0.38 g, 98%). IR (CH_2Cl_2): 1716 (C=O). ^{1}H-NMR (300 MHz, (D_6)DMSO): 2.13 (*t*, *J* = 6.5, 3 CH_2); 2.79 (*s*, 2 Me); 3.23 (*t*, *J* = 6.5, 3 CH_2); 3.31 (*s*, 3 CH_2); 7.20–8.42 (*m*, 3 CH_2, NH). ^{13}C-NMR (75 MHz, (D_6)DMSO): 42.21; 31.36; 59.32; 63.43; 66.09; 112.07; 117.03; 120.53; 124.65; 126.05; 126.42; 136.39; 148.24; 160.22; 169.67. FAB-MS: 570 (M^+).

5-(Dimethylamino)-N-*{tris[(2-{[(tris{[2-(*tert*-butoxycarbonyl)ethoxy]methyl}methyl)amino]carbonyl}-ethoxy)methyl]methyl}naphthalene-1-sulfonamide* (**13**). 1-Hydroxybenzotriazole (0.095 g, 0.70 mmol), EDCI (0.47 g, 2.5 mmol), and Et_3N (0.32 ml) were added to a soln. of **12** (0.38 g, 0.66 mmol) in 10 ml of anh. THF. Then, 5 ml of soln. of **2** [13] (1.20 g, 2.38 mmol) in anh. THF was added, and the mixture was stirred under N_2 at r.t. for 22 h. The solvent was removed under reduced pressure, and the residue was dissolved in Et_2O and washed with 0.5N HCl and brine. The Et_2O layer was dried ($MgSO_4$). The solvent was removed under vacuum, and the residue was purified by CC (SiO_2; hexane/AcOEt 1:2) to give pale blue oil (1.1 g, 82%). IR (CH_2Cl_2): 1726 (C=O, ester), 1671 (C=O, amide). ^{1}H-NMR (300 MHz, (D_6)DMSO): 1.36 (*s*, 81 H, Me); 2.08 (*t*, *J* = 6.5, 3 CH_2); 2.36 (*t*, *J* = 6.2, 9 CH_2); 2.80 (*s*, 2 Me); 3.22 (*t*, *J* = 6.5, 3 CH_2); 3.32–3.53 (*m*, 21 CH_2); 6.93 (*s*, 3 NH); 7.19–8.42 (*m*, 7 NH). ^{13}C-NMR (100 MHz, (D_6)DMSO): 28.25; 36.26; 36.63; 45.62; 60.05; 62.78; 67.24; 67.54; 68.83; 69.76; 115.36; 120.48; 123.85; 127.80; 127.90; 129.38; 129.49; 129.82; 139.83; 151.60; 170.60; 170.84. MALDI-MS: (anthracene) 2033.1 (M^+). Anal. calc. for $C_{100}H_{169}N_5O_{35}S$ (2032.13): C 59.06, H 8.38; found: C 59.16, H 8.50.

5-(Dimethylamino)-N-*(tris{[2-({tris[(2-carboxyethoxy)methyl]amino}carbonyl)ethoxy]methyl}methyl)-naphthalene-1-sulfonamide* (**14**). Compound **13** (1.0 g, 0.51 mmol) was stirred in 10 ml of 96% HCOOH under N_2 at r.t. for 20 h. The HCOOH was removed under reduced pressure, and any traces of remaining acid were removed by co-distilling with $CHCl_3$ under vacuum to give a slightly yellow foam (0.72 g, 93%). IR (CH_2Cl_2): 1640 (C=O). ^{1}H-NMR (300 MHz, (D_6)DMSO): 2.08 (*t*, *J* = 6.4, 3 CH_2); 2.40 (*t*, *J* = 6.3, 9 CH_2); 2.79 (*s*, 2 Me); 3.22 (*t*, *J* = 6.6, 3 CH_2); 3.32–3.59 (*m*, 21 CH_2); 6.97 (*s*, 3 NH); 7.19–8.42 (*m*, 7 H, NH, CH). ^{13}C-NMR (75 MHz, (D_6)DMSO): 31.72; 33.18; 42.26; 56.78; 59.42; 63.84; 64.17; 65.34; 66.33; 112.01; 117.02; 120.57; 124.52; 124.63; 126.05; 126.40; 136.31; 148.23; 167.36; 169.83. FAB-MS: 1529 ($[M+H]^+$).

5-(Dimethylamino)-N-*[tris({2-[({tris[(2-{[(tris{[2-(*tert-*butoxycarbonyl)ethoxy]methy}methyl)amino]carbonyl}ethoxy)methyl]methyl}amino)carbonyl]ethoxy}methyl)methyl]naphthalene-1-sulfonamide* (**15**). 1-Hydroxybenzotriazole (0.013 g, 0.098 mmol), EDCI (0.046 g, 0.24 mmol), and Et_3N (0.1 ml) were added to a soln. of **12** (0.039 g, 0.069 mmol) in 10 ml of anh. THF. Then, a 5-ml soln. of **4** [13] (0.50 g, 0.28 mmol) in anh. THF was added, and the mixture was stirred under N_2 at r.t. for 30 h. The solvent was removed under reduced pressure, and the residue was dissolved in Et_2O and washed with 0.5N HCl and brine. The Et_2O layer was dried ($MgSO_4$). The solvent was removed under vacuum, and the residue was purified by CC (SiO_2; MeOH/AcOEt 1:50) to give pale blue oil (0.27 g, 67%). IR (CH_2Cl_2): 1724 (C=O, ester), 1669 (C=O, amide). ^{1}H-NMR (400 MHz, (D_6)acetone): 1.33 (*s*, 27 Me); 2.10 (*t*, *J* = 7.3, 3 CH_2); 2.32–2.35 (*m*, 36 CH_2); 2.82 (*s*, 2 Me); 3.27–3.31 (*m*, 6 CH_2); 3.52–3.60 (*m*, 72 CH_2); 6.53 (br. *s*, 12 NH); 6.75 (br. *s*, NH); 7.18–8.52 (*m*, 6 CH). ^{13}C-NMR (100 MHz, (D_6)acetone): 28.84; 37.26; 38.20; 37.73; 46.45; 61.19; 61.30; 63.86; 68.33; 68.83; 66.49; 80.94; 70.15; 70.27; 80.94; 122.06; 124.91; 130.03; 130.49; 131.36; 139.83; 140.01; 141.16; 152.00; 171.85; 171.73. MALDI-MS (anthracene): 5917.9 (M^+). Anal. calc. for $C_{25}H_{34}N_2O_{11}S$ (5913.40): C 58.66, H 8.55; found: C 58.38, H 8.79.

5-(Dimethylamino)-N-*{tris({2-[({[tris({2-[({tris[(2-carboxyethoxy)methyl]methyl}amino)carbonyl]ethoxy}methyl)methyl]amino}carbonyl)ethoxy]methyl)methyl}naphthalene-1-sulfonamide* (**16**). Compound **15** (0.17 g, 0.029 mmol) was stirred in 5 ml of 96 % HCOOH under N_2 at r.t. for 24 h. The HCOOH was removed under reduced pressure, and any traces of remaining acid were removed by co-distilling with $CHCl_3$ under vacuum to give a slightly yellow foam (0.11 g, 89%). IR (CH_2Cl_2): 1651 (C=O, ester). ^{1}H-NMR (300 MHz, (D_6)acetone): 2.34 (*t*, *J* = 2.34, 3 CH_2); 2.53–2.58 (*m*, 36 CH_2); 2.90 (*s*, 2 Me); 3.37–3.52 (*m*, 6 CH_2); 3.63–3.37 (*m*, 72 CH_2); 6.95 (br. *s*, 12 NH); 7.29–8.57 (*m*, 7 H, CH, NH); ^{13}C-NMR (75 MHz, (D_6)acetone): 31.14; 33.63; 31.14; 41.72; 45.56; 47.75; 46.62; 56.96; 57.05; 59.45; 63.63; 64.24; 65.57; 111.67; 124.79; 126.31; 126.60; 136.01; 148.22; 158.17; 169.15; 169.82. MALDI-MS (α-cyano-4-hydroxycinnamic acid): 4424.8 ($[M + Na]^+$). Anal. calc. for $C_{181}H_{286}N_{14}O_{107}S \cdot 10\ H_2O$ (4579.81): C 47.44, H 6.73; found: C 47.06, H 7.02.

Benzyl N-*[Tris({2-[(*tert-*butylamino)carbonyl]ethoxy}methyl)methyl]carbamate* (**17**). 1-Hydroxybenzotriazole (0.14 g, 1.0 mmol), Et_3N (0.45 ml, 3.2 mmol), and EDCI (0.63 g, 3.3 mmol) was added to **1** [13] (0.16 g, 0.34 mmol) in 10 ml of anh. DMF. Then, (*t*-Bu)NH_2 (0.15 ml, 1.2 mmol) was added in one portion, and the mixture was stirred under N_2 for 24 h. After removal of the solvent at reduced pressure, the residue was dissolved in Et_2O and washed with 0.5M HCl and brine. The Et_2O layer was then dried ($MgSO_4$), the solvent was removed *in vacuo*, and the residue purified by CC (SiO_2; AcOEt) to yield a colorless oil, which gradually turned to white crystals on standing (0.20 g, 90%). ^{1}H-NMR (400 MHz, $CDCl_3$): 1.40 (*s*, 9 Me); 2.30 (*t*, 3 CH_2); 3.65 (*m*, 6 CH_2); 5.00 (*s*, CH_2); 5.30 (br. *s*, NH); 5.90 (br. *s*, 3 NH); 7.27–7.35 (*m*, 5 CH). ^{13}C-NMR (75 MHz, $CDCl_3$): 29.19; 38.12; 51.49; 59.18; 66.67; 67.98; 69.36; 128.48; 128.84; 136.91; 155.49; 170.82. FAB-MS: 1274 (2 M^+), 637 (M^+). Anal. calc. for $C_{33}H_{56}N_4O_8$ (636.8): C 62.24, H 8.86; found: C 61.87, H 8.85.

Benzyl N-*{Tris[(2-{[(tris{[2-carboxyethoxy]methyl}methyl)amino]carbonyl}ethoxy)methyl]methyl}carbamate* (**18**). Compound **3** [13] (1.3 g, 0.69 mmol) was stirred in 15 ml of 96% HCOOH for 18 h. Then, HCOOH was removed at reduced pressure, and any traces of remaining acid were removed by co-distilling with $CHCl_3$ and MeOH under vacuum. The product was then dried under reduced pressure at 50° to produce a colorless oil in quant. yield (0.99 g). ^{1}H-NMR (400 MHz, (D_6)acetone): 2.30 (*t*, *J* = 6.0, 3 CH_2); 2.41 (*t*, *J* = 6.0, 9 CH_2); 3.56 (*t*, *J* = 6.0, 12 CH_2); 3.60 (*s*, 12 CH_2); 4.94 (*s*, CH_2); 5.86 (br. *s*, NH); 6.68 (br. *s*, 3 NH); 7.06–7.29 (*m*, 5 CH). ^{13}C-NMR (75 MHz, (D_6)acetone): 35.63; 38.28; 60.42; 61.38; 66.89; 68.14; 68.74; 70.17; 70.43; 129.08; 129.21; 129.68; 163.03; 173.02; 173.79. FAB-MS: 1430 ($[M + H]^+$). Anal. calc. for $C_{60}H_{92}N_4O_{35} \cdot H_2O$ (1447.4): C 49.79, H 6.55; found: C 49.85, H 6.79.

2,3,6,7-Tetrahydro-11-oxo-N-*(Tris{[2-([[tris({2-[(*tert-*butylamino)carbonyl]ethoxy}methyl)methyl]amino}carbonyl)ethoxy]methyl}methyl)-1*H,5H,*11*H-*[1]benzopyrano[6,7,8*-ij*]quinolizine-9-carboxamide* (**19a**). Compound **7** (0.081 g, 0.052 mmol) was dissolved in anh. DMF (5 ml) under N_2, and cooled to 0° in an ice-water bath. 1-Hydroxybenzotriazole (0.067 g, 0.49 mmol) was added followed by EDCI (0.45 g, 2.4 mmol), and (*t*-Bu)NH_2 (0.48 ml, 4.6 mmol). The mixture was allowed to reach r.t. slowly and stirred for 66 h under N_2. Then, DMF was distilled off under reduced pressure at 35°. The residue was dissolved in CH_2Cl_2 and washed with 0.5M HCl and brine. The org. layer was dried ($MgSO_4$), filtered, and the solvent was evaporated *in vacuo*. The residue was washed three times with benzene and dried under vacuum for 2 d, to yield a hygroscopic, brown solid (0.063 g, 59%). ^{1}H-NMR (300 MHz, $CDCl_3$): 1.34 (*s*, 27 Me); 1.98 (*m*, 2 CH_2); 2.34 (*t*, *J* = 7.7, 9 CH_2); 2.45 (*t*, *J* = 8.0, 3 CH_2); 2.80 (*m*, 2 CH_2); 3.33 (*m*, CH_2); 3.69 (*m*, 21 CH_2); 3.86 (*s*, 3 CH_2); 6.48 (br. *s*, 9 NH); 6.59 (br. *s*, 3 NH); 7.07 (*s*, CH); 8.52 (*s*, CH); 9.18 (br. *s*, NH). ^{13}C-NMR (75 MHz, $CDCl_3$): 20.14; 37.57; 51.03; 59.86; 60.24; 67.64; 67.82; 69.09; 69.43; 108.15; 109.18; 119.90; 152.71; 163.26; 170.63; 171.32. MALDI-MS (anthracene): 2057.8 (M^+), 2157.9 ($[M - {}^t$BuNH + $C_8H_{18}N_3O]^+$), 2257.8 ($[M - 2\ {}^t$BuNH + 2 $C_8H_{18}N_3O]^+$).

Benzyl N-*(Tris{[2-({[tris({2-[(*tert*-butylamino)carbonyl]ethoxy}methyl)methyl]amino}carbonyl)ethoxy]-methyl}methyl)carbamate* (**19b**). 1-Hydroxybenzotriazole (0.13 g, 0.99 mmol) and DIC (0.56 ml, 3.6 mmol) were added to **18** (0.15 g, 0.11 mmol) in 10 ml of anh. THF under N_2, and the mixture was stirred for 12 h. (*t*-Bu)NH_2 (0.35 ml, 3.3 mmol) was then added, and the mixture was stirred under N_2 for an additional 24 h. After removal of the solvent at reduced pressure, the residue was dissolved in Et_2O and washed with 0.5M HCl and brine. The Et_2O layer was then dried ($MgSO_4$), the solvent was removed *in vacuo*, and the residue purified by CC (SiO_2; AcOEt/MeOH 4:1) to yield a colorless oil (0.17 g, 78%). ^{1}H-NMR (300 MHz, $CDCl_3$): 1.27 (*s*, 27 Me); 2.26 (*t*, $J = 5.8$, 9 CH_2); 2.38 (*t*, $J = 6.0$, 3 CH_2); 3.55–3.63 (*m*, 24 CH_2); 4.96 (*s*, CH_2); 5.57 (br. *s*, NH); 6.39 (br. *s*, NH); 6.69 (br. *s*, 3 NH); 7.22–7.28 (*m*, 5 CH). ^{13}C-NMR (75 MHz, $CDCl_3$): 29.23; 37.53; 37.73; 51.36; 59.38; 60.27; 66.67; 67.97; 68.13; 69.63; 70.22; 128.34; 128.46; 128.87; 130.12; 156.19; 170.63; 169.77. FAB-MS: 1947 ($[M + Na]^+$), 1925 ($[M + H]^+$).

Coupling the Fluorescent Dendrimers and Dyes to the Resin. A typical procedure used 0.250 g of *ArgoGel*-NH_2 (0.43 mmol/g), to be swollen in 2 ml of anh. DMF, in a 10-ml fritted polypropylene *PD-10* column (*Pharmacia Biotech*) used as a reaction vessel. Then, for every equiv. of NH_2, 3 equiv. of acid and 3 equiv. of HOBT were dissolved in 4 ml of DMF. This soln. was added to the resin, followed by 50 equiv. of DIC. The mixture was slowly rotated in a rotisserie mixer for 5 h at r.t. Then, 10 equiv. of (*t*-Bu)NH_2 were added, and the mixing was continued for 18 h. At this point, the resin was washed with THF (3×), MeOH (3×), H_2O (3×), MeOH (3×), and THF (3×). Each washing took 20 min. Then, the beads were dried under vacuum for 18 h over P_2O_5.

The control beads, **26**–**29**, were prepared in the same fashion, but CH_2Cl_2 was used instead of DMF because of solubility problems with **5**. These reactions were performed in standard glassware with flea stirrers. The 10% coumarin resin, **28**, was prepared from **5** and cyclohexanecarboxylic acid (3 equiv. of total acid) in a 1:9 ratio, resp. The 4% diluted coumarin resin, **29**, was prepared as described above, but in a 1:27 ratio of coumarin to cyclohexanecarboxylic acid, respectively.

The G2, **20**, and G3, **22**, coumarin beads were further modified with rhodamine B to afford **24** and **25**. Beads **20** and **22** were swollen in 2 ml of DMF. Then, on the assumption that these beads still had a 0.43 mmol/g loading, 3 equiv. of a DMF soln. of rhodamine B isothiocyanate and cyclohexyl isothiocyanate, in a 1:27 ratio, were added. The mixture was rotated in a rotisserie mixer for 18 h. Then, the washing and drying process was as described above.

Procedure for the Microtome Slicing. Beads were embedded in *Surgipath Blue Ribbon* paraffin and sliced on a *Leica RM 2125* microtome with a *Sakura Finetek Accu-Edge* high-profile blade. The slices were mounted on *Surgipath Precleaned Snowcoat Xtra* 25 mm × 75 mm × 1.0 mm-glass microscope slides.

Modified beads were distributed evenly on the bottom of a heated (55°) 1-cm^2 metal mold. The mold was then filled with melted paraffin at 55° and left standing for 10 min at 55° to allow beads to sink to the bottom of the mold and the trapped air to escape. If air bubbles were still present, the beads were manipulated with heated

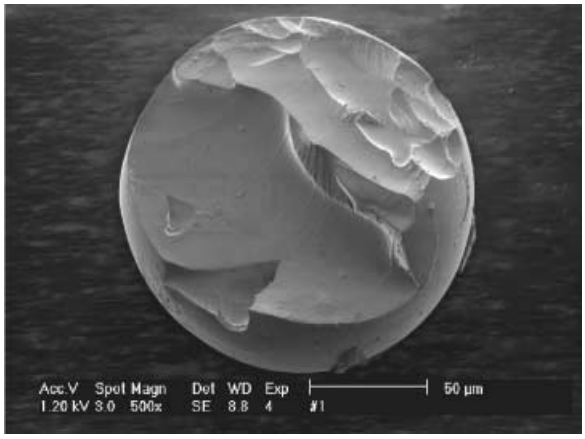

Fig. 13. *ESEM Image of a microtome-sliced bead of uneven thickness.* Note the large section of spherical surface in the lower right.

forceps to release the air bubbles. The molds were covered with a microtome mounting plate and placed in a freezer at $-25°$ for 15 min. After cooling, the mold was removed, and the plate was immediately mounted on a *Leica* microtome equipped with a high-profile blade. Slices of 4 ± 1-μm thickness were obtained strung into paraffin ribbons, which were expanded with a 40° water flotation bath. The ribbons were lifted from the bath and mounted on microscope slides. The slides were placed in an oven at 85° for 15 min to dry the slide and allow the slices to settle onto the surface of the slide. The paraffin was removed by subsequent treatment with toluene or xylene (3×10 min). Microtome slicing of the beads was very destructive, and the majority of slices were partially cut, fragmented, or otherwise severely damaged during the process (*Fig. 13*). The slices were visually inspected for uniform thickness and diameter by the addition of a drop of toluene to the slide, so the slices could be carefully manipulated and then removed and remounted onto another slide for photography or electron microscopy.

REFERENCES

[1] V. V. Narayanan, G. R. Newkome, *Top. Curr. Res.* **1998**, *197*, 19; G. R. Newkome, C. N. Moorefield, F. Vögtle, 'Dendritic Macromolecules: Concepts, Synthesis, and Perspectives' VCH, Weinheim, Germany, 1996; G. R. Newkome, C. N. Moorefield, in 'Comprehensive Supramolecular Chemistry', Ed. D. N. Reinhoudt, Elsevier Sciences, New York, 1996, Vol. 10; D. A. Tomalia, H. D. Durst, *Top. Curr. Chem.* **1993**, *165*, 193; D. A. Tomalia, A. D. Naylor, A. Goddard, *Angew. Chem., Int. Ed. Engl.* **1990**, *29*, 138.

[2] a) S. Hecht, J. M. J. Fréchet, *Angew. Chem., Int. Ed.* **2001**, *40,* 74; b) C. B. Gorman, J. C. Smith, *Acc. Chem. Res.* **2001**, *34*, 60; c) C. M. Cardona, S. Mendoza, A. E. Kaifer, *Chem. Soc. Rev.* **2000**, *29*, 37; d) D. K. Smith, F. Diederich, *Top. Curr. Chem.* **2000**, *210,* 183; e) A. W. Bosman, H. M. Janssen, E. W. Meijer, *Chem. Rev.* **1999**, *99,* 1665; f) M. Fisher, F. Vögtle, *Angew. Chem., Int. Ed.* **1999**, *38,* 884; g) D. K. Smith, F. Diederich, *Chem. – Eur. J.* **1998**, *4,* 1353; h) F. Zeng, S. C. Zimmerman, *Chem. Rev.* **1997**, *97,* 1681.

[3] C. M. Cardona, J. Alvarez, A. E. Kaifer, T. D. McCarley, S. Pandey, G. A. Baker, N. J. Bonzagni, F. V. Bright, *J. Am. Chem. Soc.* **2000**, *122,* 6139; C. M. Cardona, T. D. McCarley, A. E. Kaifer, *J. Org. Chem.* **2000**, *65,* 1857; F. Vögtle, M. Plevoets, M. Nieger, G. C. Azzellini, A. Credi, L. De Cola, V. De Marchis, M. Venturi, V. Balzani, *J. Am. Chem. Soc.* **1999**, *121,* 6290; J. Issberner, F. Vögtle, L. De Cola, V. Balzani, *Chem. – Eur. J.* **1997**, *3*, 706.

[4] S. E. Stiriba, H. Frey, R. Haag, *Angew. Chem., Int. Ed.* **2002**, *41*, 1329; N. Rockendorf, T. K. Lindhorst, *Top. Curr. Chem.* **2001**, *217,* 201; C. M. Casado, I. Cuadrado, M. Morán, B. Alonso, B. García, B. González, J. Losada, *Coord. Chem. Rev.* **1999**, *53*, 185.

[5] a) F. H. Ling, V. Lu, F. Svec, J. M. J. Fréchet, *J. Org. Chem.* **2002**, *67,* 1993; b) C. Chi, J. Wu, X. Wang, Z. Zhao, J. Li, F. Wang, *Macromolecules* **2001**, *34,* 3812; c) R. Haag, *Chem. – Eur. J.* **2001**, *7,* 327; d) S. Lebreton, S. Monaghan, M. Bradley, *Aldrichimica Acta* **2001**, *34(3)*, 75; e) A. Basso, B. Evans, N. Pegg, M. Bradley, *Chem. Commun.* **2001**, 697; f) A. Basso, B. Evans, N. Pegg, M. Bradley, *Tetrahedron Lett.* **2000**, *41*, 3763; g) S. C. Bourque, H. Alper, L. E. Manzer, P. Arya, *J. Am. Chem. Soc.* **2000**, *122*, 956; h) P. Arya, N. V. Rao, J. Singkhonrat, H. Alper, C. Bourque, L. E. Manzer, *J. Org. Chem.* **2000**, *65,* 1881; i) A. Mahajan, S. R. Chhabra, W. C. Chan, *Tetrahedron Lett.* **1999**, *40*, 4909; j) V. Swali, N. J. Wells, J. Langley, M. Bradley, *J. Org. Chem.* **1997**, *62*, 4902.

[6] D. Seebach, A. K. Beck, A. Heckel, *Angew. Chem.* **2001**, *113*, 96; *Angew. Chem., Int. Ed.* **2001**, *40,* 92.

[7] H. Sellner, P. B. Rheiner, D. Seebach, *Helv. Chim. Acta* **2002**, *85*, 352; P. B. Rheiner, D. Seebach, *Chem. – Eur. J.* **1999**, *5*, 3221; H. Sellner, D. Seebach, *Angew. Chem., Int. Ed.* **1999**, *38*, 1918; P. B. Rheiner, H. Sellner, D. Seebach, *Helv. Chim. Acta* **1997**, *80*, 2027.

[8] H. Sellner, J. K. Karjalainen, D. Seebach, *Chem. – Eur. J.* **2001**, *7*, 2873; H. Sellner, C. Faber, P. B. Rheiner, D. Seebach, *Chem. – Eur. J.* **2000**, *6*, 3692.

[9] R. E. Gawley, Q. Zhang, P. I. Higgs, S. Wang, R. M. Leblanc, *Tetrahedron Lett.* **1999**, *40,* 5461, corrigendum 6135; P. Kele, J. Orbulescu, T. L. Calhoun, R. E. Gawley, R. M. Leblanc, *Tetrahedron Lett.* **2002**, in press; R. E. Gawley, S. Pinet, C. M. Cardona, P. K. Datta, T. Ren, W. C. Guida, J. Nydick, R. M. Leblanc, **2002**, submitted.

[10] G. M. Lipkind, H. A. Fozzard, *Biophys. J.* **1994**, *66*, 1.

[11] G. R. Newkome, X. Lin, *Macromolecules* **1991**, *24*, 1443; G. R. Newkome, X. Lin, J. K. Young, *Synlett* **1992**, 53; G. R. Newkome, R. K. Behera, C. N. Moorefield, G. R. Baker, *J. Org. Chem.* **1991**, *56*, 7162; C. N.

Moorefield, G. R. Newkome, in 'Advances in Dendritic Macromolecules', Ed. G. R. Newkome, JAI Press, Greenwich, 1994, Vol. 1.
[12] B. Yan, P. C. Martin, J. J. Lee, *Com. Chem.* **1999**, *1*, 78.
[13] C. M. Cardona, R. E. Gawley, *J. Org. Chem.* **2002**, *67*, 1411.
[14] J. Rademann, M. Barth, R. Brock, H. J. Egehaaf, G. Jung, *Chem. – Eur. J.* **2001**, *7*, 3884.
[15] G. T. Copeland, S. J. Miller, *J. Am. Chem. Soc.* **1999**, *121,* 4306.
[16] R. A. Farrer, G. T. Copeland, M. J. R. Previte, M. M. Okamoto, S. J. Miller, J. T. Fourkas, *J. Am. Chem. Soc.* **2002**, *124*, 1994.
[17] S. R. McAlpine, C. W. Lindsley, J. C. Hodges, D. M. Leonard, G. F. Filzen, *J. Comb. Chem*. **2001**, *3*, 1; S. R. McAlpine, S. L. Schreiber, *Chem. – Eur. J.* **1999**, *5*, 3528.
[18] M. H. J. Ohlmeyer, R. N. Swanson, L. W. Dillard, J. C. Reader, G. Asouline, R. Kobayashi, M. Wigler, W. C. Still, *Proc. Natl. Acad. Sci. U.S.A.* **1993**, *90*, 10922; H. P. Nestler, P. A. Bartlett, W. C. Still, *J. Org. Chem.* **1994**, *59*, 4723.
[19] L. A. Carpino, H. Imazumi, A. El-Faham, F. J. Ferre, C. Zhang, Y. Lee, B. M. Foxman, P. Henklein, C. Hanay, C. Mügge, H. Wenschuh, J. Klose, M. Beyermann, M. Bienert, *Angew. Chem., Int. Ed.* **2002**, *41*, 442; L. A. Carpino, *J. Am. Chem. Soc.* **1993**, *115*, 4397.

Received May 31, 2002